OPEN ACCESS

ORIGINAL RESEARCH

SUMO pathway inhibition targets an aggressive pancreatic cancer subtype

Alexander Biederstädt,[1] Zonera Hassan ,[2] Christian Schneeweis,[2] Markus Schick,[3] Lara Schneider,[4,5] Alexander Muckenhuber,[6] Yingfen Hong,[1] Gerrit Siegers,[1] Lisa Nilsson,[7] Matthias Wirth,[3] Zahra Dantes,[2] Katja Steiger,[6,8] Kathrin Schunck,[9] Steve Langston,[10] H-P Lenhof,[4] Andrea Coluccio,[2,11] Felix Orben,[2] Jolanta Slawska,[1] Anna Scherger,[1] Dieter Saur,[8,11] Stefan Müller,[9] Roland Rad,[8,12] Wilko Weichert,[6,8] Jonas Nilsson,[7] Maximilian Reichert ,[2,8] Günter Schneider ,[2,8] Ulrich Keller [3,8]

► Additional material is published online only. To view please visit the journal online (http://dx.doi.org/10.1136/gutjnl-2018-317856).

For numbered affiliations see end of article.

Correspondence to
Dr Günter Schneider, Medical Clinic and Polyclinic II, Klinikum rechts der Isar, TU Munich, 81675 Munich, Germany; guenter.schneider@tum.de and Professor Ulrich Keller, Department of Hematology, Oncology and Tumor Immunology, Campus Benjamin Franklin, Charité - Universitätsmedizin Berlin, 12203 Berlin, Germany; ulrich.keller@charite.de

AB, ZH, CS and MS are joint first authors.
GS and UK are joint senior authors.

Received 2 November 2018
Revised 20 December 2019
Accepted 22 December 2019
Published Online First 30 January 2020

To cite: Biederstädt A, Hassan Z, Schneeweis C, *et al*. *Gut* 2020;**69**:1472–1482.

ABSTRACT

Objective Pancreatic ductal adenocarcinoma (PDAC) still carries a dismal prognosis with an overall 5-year survival rate of 9%. Conventional combination chemotherapies are a clear advance in the treatment of PDAC; however, subtypes of the disease exist, which exhibit extensive resistance to such therapies. Genomic MYC amplifications represent a distinct subset of PDAC with an aggressive tumour biology. It is clear that hyperactivation of MYC generates dependencies that can be exploited therapeutically. The aim of the study was to find and to target MYC-associated dependencies.

Design We analysed human PDAC gene expression datasets. Results were corroborated by the analysis of the small ubiquitin-like modifier (SUMO) pathway in a large PDAC cohort using immunohistochemistry. A SUMO inhibitor was used and characterised using human and murine two-dimensional, organoid and in vivo models of PDAC.

Results We observed that MYC is connected to the SUMOylation machinery in PDAC. Components of the SUMO pathway characterise a PDAC subtype with a dismal prognosis and we provide evidence that hyperactivation of MYC is connected to an increased sensitivity to pharmacological SUMO inhibition.

Conclusion SUMO inhibitor-based therapies should be further developed for an aggressive PDAC subtype.

Significance of this study

What is already known on this subject?

► Current data demonstrate that certain subtypes of pancreatic ductal adenocarcinoma (PDAC) are completely resistant to clinically used chemotherapies.

What are the new findings?

► We describe for the first time the relevance of the SUMOylation pathway, linked to a poorly differentiated phenotype with a poor prognosis. PDACs with activation of the small ubiquitin-like modifier (SUMO) pathway overlap the basal-like subtype.
► We detected a cosegregation of the SUMO pathway with MYC and observed a functional relationship between both pathways.
► We demonstrate the relevance of the SUMO pathway as a therapeutic target by the use of novel SUMO-activating enzyme subunit pathway inhibitors and show that MYC hyperactivation sensitises PDAC cells towards such therapies.

How might it impact on clinical practice in the foreseeable future?

► SUMO pathway inhibitor-based therapies might be a potential approach to target a PDAC subtype.

INTRODUCTION

Pancreatic ductal adenocarcinoma (PDAC) remains a cancer with dismal prognosis reflected by a 5-year survival rate of only 9%.[1] In contrast to the continuously increasing understanding of molecular and genetic alterations of the disease,[2 3] therapies are not satisfying. Stratified molecular mechanism-based therapies are currently emerging[4] but are not standard of care for the majority of patients.

Disease stratification efforts of PDAC demonstrate the existence of several subtypes with unique biology, phenotypes and therapeutic vulnerabilities.[5–14] Such insights indicate that defining subtype-specific dependencies will allow for stratification and precise molecularly informed therapeutic intervention. These considerations are furthermore supported by retrospective investigations[15] or the COMPASS (NCT02750657) trial,[16] which demonstrate that response to conventional chemotherapies differs among subtypes of PDAC.

By controlling genes involved in ribosome biogenesis, metabolism, cell cycle and growth, the *MYC* oncogene is a driver in a subset of PDACs.[17–19] Supported by unbiased synthetic lethality screens,[20] it is clear that cancers with a hyperactive MYC network are characterised by dependencies, which offer the unique possibility for therapeutic intervention.[17 18] In line with this idea, MYC was recently demonstrated to predict responsiveness

of PDAC patient-derived xenotransplants or organoids to BET inhibitors.[21 22]

Considering the high potential of MYC to act as a marker for patient and therapy selection,[18] we set up experiments to decipher dependencies in the subgroup of PDAC with high MYC activity. We observed cosegregation of MYC with the SUMOylation machinery that is connected to sensitivity towards a specific small ubiquitin-like modifier (SUMO) inhibitor.

METHODS

Compounds, characterisation of SUMO inhibitors, and chemicals

ML-792 and ML-93 were synthesised by Millennium Pharmaceuticals/Takeda (Cambridge, Massachusetts, USA). Biochemical and cellular characterisation of ML-93 activity is described in online supplementary materials and methods (SM&M). 4-hydroxytamoxifen (4-OHT) was purchased from Sigma (Sigma, Munich, Germany).

Cell culture and cell line engineering

Description is included in SM&M.

Generation of patient-derived PDAC organoids and primary-dispersed cell lines

Primary patient-derived PDAC three-dimensional (3D) organoids were generated from primary resected human PDAC surgical specimen according to the Tuveson protocol described in[23] and in the SM&M.[24] Generation and culturing of primary-dispersed human PDAC cells is described in[25] and SM&M. Written informed consent from the patients for research use was obtained prior to the investigation.

Viability assays, SUMO inhibitor (SUMOi) treatment, clonogenic assay, annexin V, cell cycle-FACS, viability analysis by FACS, competitive repopulation assay, Western blotting and RNA isolation and expression analysis.

Description is included in SM&M.

Generation of in vivo xenografts and SUMOi toxicity

All animal experiments were performed in accordance with regional Gothenburg University animal ethics committee approval 100/16 and 5.8.18-01949/2018 and approval of Regierung von Oberbayern ROB-55.2–2532.Vet_02-17-230. A detailed description can be found in the SM&M section.

RNA-seq analysis, gene expression profiling, gene set enrichment analysis (GSEA), transcriptomics and genomics data analysis

Description is included in SM&M.

Clinical PDAC patient cohort, histological analysis and immunohistochemistry

Tissue microarrays and analysis of human PDAC cohort (n=262) are described in SM&M. The use of this tumour cohort for biomarker analysis has been approved by the Charité University ethics committee (EA1/06/2004).

Proteome analysis by mass spectrometry

Proteome analysis is described in detail in SM&M.

Statistical methods

Analysis of variance or two-sided t-test was used. P values were corrected according to Bonferroni for multiple testing. Values were calculated with GraphPad Prism6/8. P values are indicated or represented with: *p<0.05, **p<0.01, ***p<0.001, ****p<0.0001. Data are presented as mean and SD.

RESULTS

MYC is connected to the sumoylation pathway in PDAC

A recent study demonstrated that amplification of *MYC* is the sole copy number variation (CNV) associated with poor prognosis in PDAC.[26] To further substantiate these findings, we assessed TCGA-PAAD data. Twelve per cent of PDACs in this dataset harbour *MYC* amplifications connected to reduced overall survival and disease-free survival (figure 1A). Using GSEA via the GeneTrail2 1.6 web service, which uses an unweighted GSEA methodology,[27] we detected activation of the MYC network in *MYC*-amplified cancers (figure 1B). Following the concept that hyperactivity of the MYC network is connected to specific dependencies in PDAC,[17 18] we analysed further pathways active in *MYC*-amplified cancers (online supplementary table S1). We detected significant enrichment of Reactome signatures linked to protein SUMOylation as well as curated core SUMO pathways in *MYC*-amplified PDACs (figure 1C,D). Since the SUMO pathway was found to be an MYC-associated dependency in an unbiased genome-wide genetic screen in human mammary epithelial cells (HMECs),[28] an observation which could also be made in other neoplasms such as B-cell lymphomas,[29] we explored the possibility that the SUMO pathway confers a vulnerability in PDAC with hyperactivity of MYC. SUMO modification of cellular proteins is an important post-translational modification (PTM) that regulates function, localisation, interaction and expression of proteins. PTM by SUMOs has been reported to play various important roles in tumourigenesis.[30] Analogous to ubiquitination, SUMO1, SUMO2 or SUMO3 are transferred to lysine residues of proteins in a multistep catalytic process involving the E1 activating enzymes SUMO-activating enzyme subunit 1 (SAE1) and 2 (UBA2/SAE2), the E2 conjugating enzyme UBE2I (UBC9) and SUMO E3 ligases.[30 31] Next-generation sequencing data[26] demonstrated *MYC* amplifications as well as CNVs of the SUMO pathway genes *SAE1* and *UBE2I* (figure 1E), furthermore underscoring the importance of both pathways in PDAC.

Relevance of the sumoylation pathway in PDAC

To further investigate the relevance of the SUMOylation pathway, we compared the expression profiles of 69 PDACs to 61 adjacent non-tumour tissue samples[32] and observed an increased expression of the SUMO pathway components *SAE1*, *UBE2I*, *SUMO1*, *SUMO2* and *SUMO3* in PDAC (online supplementary figure S1A), underlined by a corresponding enrichment of SUMO-related gene sets in PDAC (online supplementary figure S1B). Analysing the TCGA clinical data set demonstrated that high expression of *UBE2I* is linked to a worse prognosis (figure 2A), an observation valid also for *SUMO1* (figure 2B). The Kaplan-Meier curves for PDAC with high and low *SUMO2* and *SUMO3* mRNA levels are depicted in figure 2C,D. Comparing the *UBE2I* high and low groups by GSEA demonstrated the enrichment of MYC signatures in *UBE2I* high PDACs (figure 2E). MYC signatures were also detected in PDACs with high expression of *SUMO1*, *SUMO2* and *SUMO3* mRNA (online supplementary figure S1C), again corroborating the connection of both pathways. To further stress the significance of the core SUMOylation pathway for PDAC, we analysed an additional PDAC mRNA expression

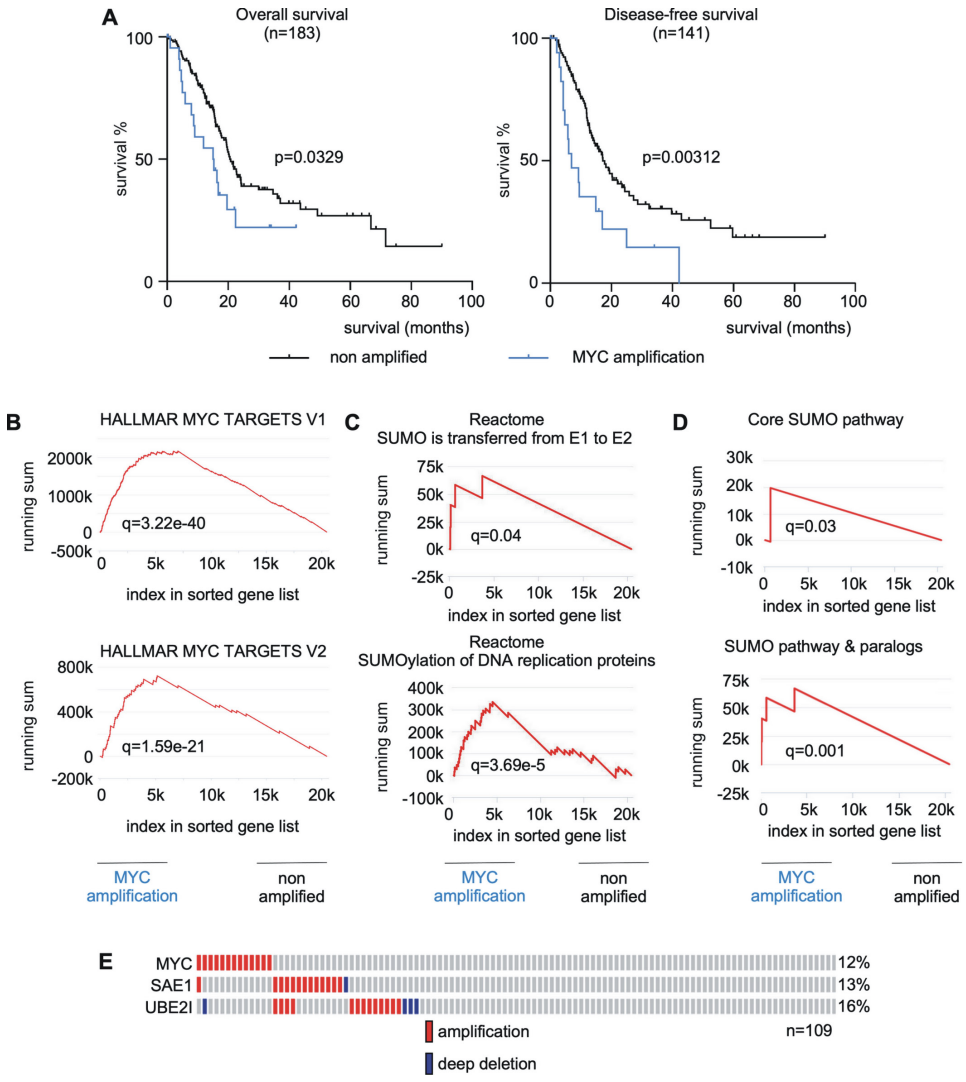

Figure 1 MYC is connected to the SUMOylation pathway in PDAC. (A) genomic *MYC* amplification (23/183 cases, 12%) is correlated with inferior overall survival (OS) (median OS 15.11 vs 20.83 months; n=183; p=0.033) and disease-free survival in PDAC (median DFS 7 vs 17.28 months; n=141; p=0.003) (data are based on the TCGA-PAAD dataset). (B) Unweighted GSEA using gene Trail2 1.6 comparing *MYC* amplified and non-amplified PDACs. q values are depicted. (C, D) Unweighted GSEA using gene Trail2 1.6 reveals significant enrichment of gene sets involved in protein sumoylation within the *MYC* amplified PDAC subgroup. Enrichment analysis was performed for published Reactome pathways (C), SUMO is transferred from E1 to E2 (UBE2I, Ubc9); sumoylation of DNA replication proteins and manually curated core SUMO pathway gene sets (D), core SUMO pathway *SAE1*, *UBA2*, *UBE2I*; SUMO pathway and paralogs *SAE1*, *UBA2*, *UBE2I*, *SUMO1*, *SUMO2*, *SUMO3*. q values are depicted. (E) Published genomics data from whole exome sequencing of 109 microdissected pancreatic cancer cases[26] demonstrates a tendency towards mutual exclusivity in genomic *MYC* and SUMO pathway components (*SAE1*, *UBE2I*) aberrations. GSEA, gene set enrichment analysis; PDAC, pancreatic ductal adenocarcinoma; SAE1, SUMO-activating enzyme subunit 1; SUMO, small ubiquitin-like modifier.

dataset from 96 patients,[7] where we detected a human PDAC subtype with increased expression of core SUMO pathway genes (SUMO^{high}) (figure 2F). Comparing the SUMO^{high} subtype with the SUMO^{low} subtype by the GeneTrail2 demonstrated enrichment of MYC signatures (online supplementary figure S1D). A complete list of pathways active in the SUMO^{high} subtype is listed in online supplementary table S2. Also in this human PDAC dataset, the SUMO^{high} PDACs were characterised by decreased progression-free as well as overall survival (online supplementary figure S1E). PDAC subtyping efforts have shown the existence of several subtypes and squamous/basal-like/quasi-mesenchymal, classic/progenitor, immunogenic and aberrantly differentiated endocrine exocrine-subtypes were described, although not all of these subtypes were found to be stable/reproducible.[33] The recurrently identified and therefore currently generally accepted squamous/basal-like/quasi-mesenchymal subtype carries the worst prognosis.[5–8 10 12] SUMO^{high} PDACs are characterised by an enrichment of squamous subtypes (figure 2F,G) and poorly or undifferentiated tumours (figure 2F, H).

To further substantiate the relevance of the SUMOylation pathway in PDAC, we analysed SUMO1, and SUMO2/3 expression in an additional human PDAC cohort (n=262) at the protein level using immunohistochemistry (IHC). Here, we observed PDACs with low, intermediate or high SUMO1 and SUMO2/3 expression (figure 2I). Consistent with the RNA expression-based analysis, the SUMO1-high phenotype was associated with less differentiated tumours (figure 2J). In addition, we detected a connection of high SUMO1 expression to younger patients (figure 2K) and female gender (figure 2L). Multivariate survival analysis demonstrated a connection of

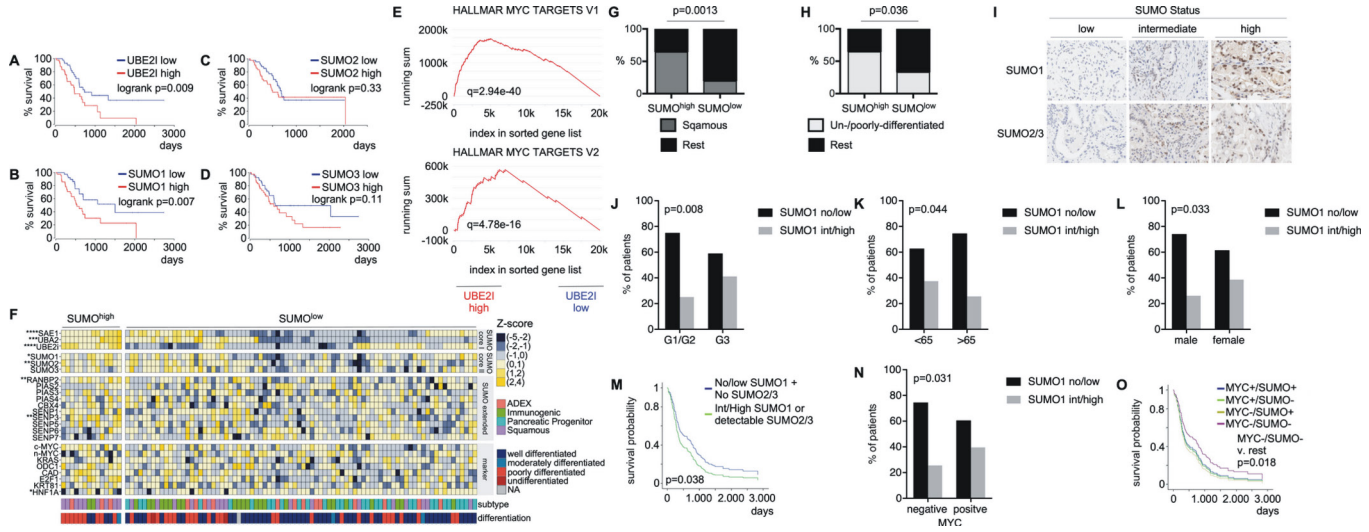

Figure 2 SUMOylation components are induced in PDAC and associated with adverse prognosis. (A–D) Transcriptomics data (TCGA-PAAD) was analysed for correlation of SUMO pathway component transcript levels and survival rates. Overall survival of patients with high expression of *UBE2I, SUMO1, SUMO2* or *SUMO3* mRNA (>75th percentile) was compared with overall survival of patients with low mRNA expression of these genes (<25th percentile). High expression of *UBE2I* and *SUMO1* mRNA is significantly associated with decreased overall survival. P value of a logrank test is depicted. All survival curves were directly retrieved via the OncoLnc platform (http://www.oncolnc.org/) using the above defined thresholds. (E) Unweighted GSEA of *UBE2I*-high and low groups using gene Trail2 1.6 reveals significant enrichment of MYC hallmark target genes within *UBE2I*-high subgroup (thresholds defined in A–D). Q value is depicted. (F) Manual curation of a publicly available gene expression dataset of PDAC patients (n=96)[7] was used to define a SUMO-high population, characterised by positive z-scores for *SAE1*, *UBA2* and *UBE2I* (n=14). (G, H) SUMO high PDACs corresponding to 2F were analysed for association with tumour differentiation or subtype. (G) Enrichment of the squamous subtype and (H) enrichment of undifferentiated and poorly differentiated tumours in the SUMO high subtype. P values of a Fisher's exact test are indicated. (I) Representative IHC staining of surgical PDAC specimen (n=262) with low, intermediate and high SUMO1 or SUMO2/3 expression. (J–L) Nuclear SUMO1 expression is significantly enriched in biologically aggressive G3 tumours as well as in younger patients, that is, <65 years of age and female patients. The P values of a Pearson's X^2 test are depicted. G1: well differentiated, G2: moderately differentiated, G3: poorly differentiated PDAC. (M) Combined SUMO1 and SUMO2/3 nuclear expression as measured by IHC is correlated with an adverse prognosis in PDAC patients. The p value of a logrank test is shown. (N) MYC IHC was conducted in the above-described PDAC cohort. PDACs were grouped in tumours with positive and negative MYC staining and connected to the SUMO1 status. The p value of a Pearson's X^2 test is depicted. (O) A multivariate analysis reveals a prognostically favourable subpopulation of patients with low MYC-/SUMO expression that exhibits the best clinical course (p=0.018, logrank) independent of initial Union for International Cancer Control (UICC) stage. GSEA, gene set enrichment analysis; IHC, immunohistochemistry; PDAC, pancreatic ductal adenocarcinoma; SEA1, SUMO-activating enzyme subunit 1; SUMO, small ubiquitin-like modifier.

the SUMOylation pathway to reduced survival (figure 2M). To further demonstrate the connection of the SUMO pathway to MYC, we analysed MYC protein expression using IHC in the same cohort. MYC positive tumours were significantly enriched in the SUMO1 high phenotype (figure 2N). Furthermore, multivariate analysis reveals that survival of patients belonging to the $MYC^{low}/SUMO^{low}$ subtype is significantly better compared with all other subgroups (figure 2O). Together, mRNA and protein expression data in large human PDAC cohorts demonstrate that the SUMOylation pathway characterises a subset of poorly differentiated PDACs with a significant enrichment of squamous/basal-like tumours. Furthermore, a subset of PDAC coactivates the SUMO pathway and MYC.

MYC connects to the SUMOylation pathway in PDAC cells

To additionally analyse the connection of MYC to the SUMOylation pathway, we used human PDAC cell lines, where we detected a positive correlation of *MYC* mRNA with the expression of *SUMO1* (p=0.01) and *SUMO2* (p=0.09) mRNA (figure 3A). A positive correlation of the *MYC* mRNA to genes of the SUMO pathway was also detected in murine PDAC cell lines (online supplementary figure S2A). We quantified MYC protein expression in ten human PDAC cell lines (figure 3B,C). Higher MYC expression was connected to higher levels of total SUMO1 and SUMO2/3 conjugated proteins (figure 3D). To demonstrate the induction of the SUMO pathway by MYC in human PDAC cell lines, we used an MYC oestrogen receptor fusion protein (MYC^{ER}) in IMIM-PC1 cells (figure 3E), which express low levels of MYC (figure 3B,C). Activation of MYC by 4-OHT treatment induced the expression of classical MYC target genes including *ODC1* and *CAD* (figure 3F). In RNA-seq experiments, we observed MYC signatures activated on 4-OHT treatment (figure 3G), demonstrating the anticipated activation of the MYC network. Signatures connected to the SUMO pathway were coactivated on 4-OHT treatment (figure 3H and online supplementary table S3). In addition to these gain-of-function data, we analysed RNA-seq data, in which MYC was potently inhibited in murine PDAC cells using a dominant-negative form of MYC, called OmoMYC.[34] OmoMYC coinhibited the MYC network and signatures connected to the SUMO pathway (online supplementary figure S2B). In addition, we transduced murine PDAC cells with vectors driving the expression of GFP or MYC together with GFP (figure 3I,J). In GSEA of RNA-seq of these cells, we detected the activation of the MYC pathway (figure 3K) and signatures connected to SUMOylation (figure 3L). A slight increase in protein SUMOylation was observed in SUMO1 and SUMO2/3 western blots in MYC overexpressing cells (figure 3M). The GO_PROTEIN_SUMOYLATION signature contains the core SUMO pathway genes *Sumo1-3*, *Sae1*, *Sae2/Uba2* and *Ube2i*, which were upregulated in MYC overexpressing PPT-53631 cells comparable to MYC target genes

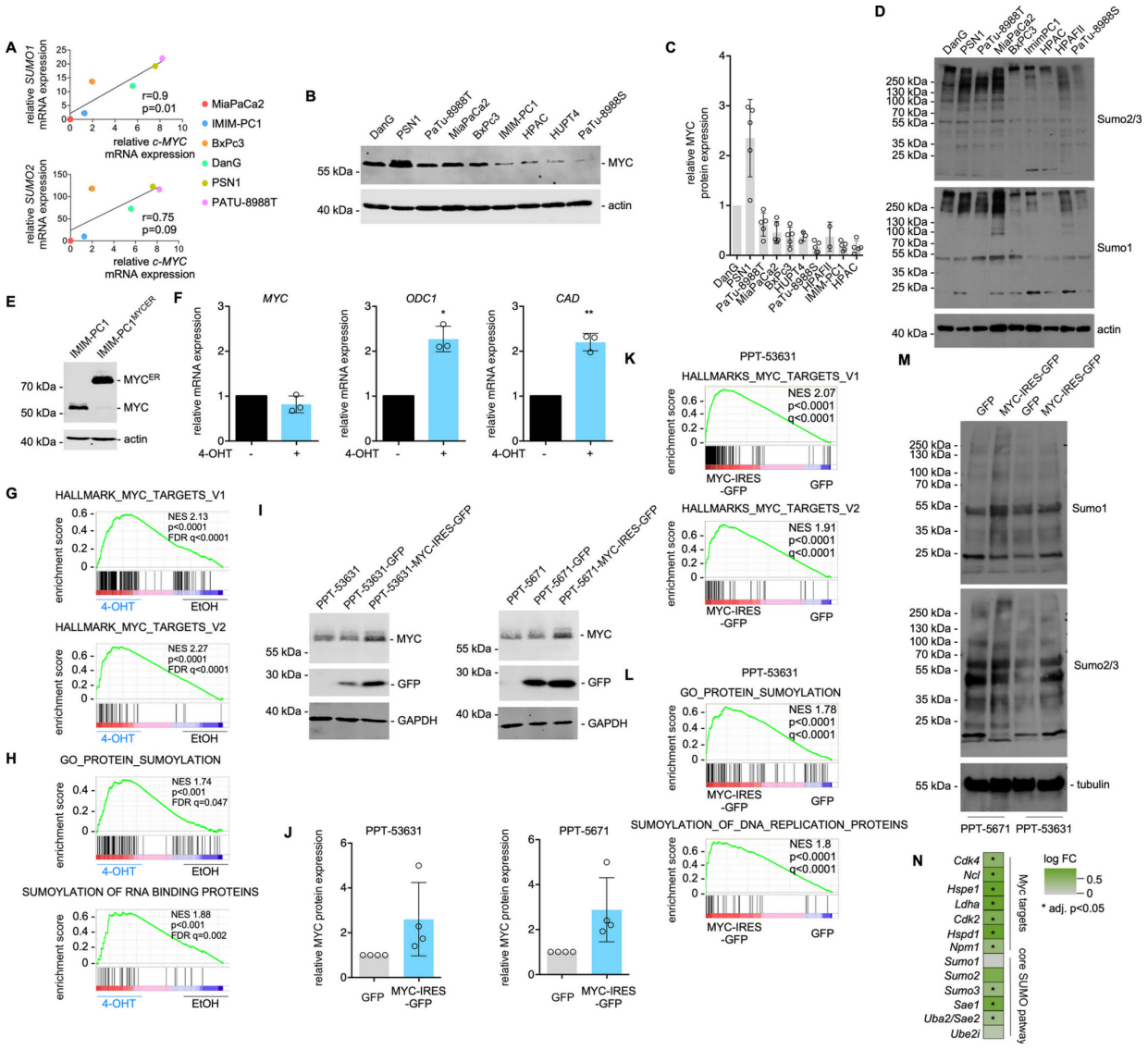

Figure 3 MYC activation induces SUMOylation pathway components. (A) *SUMO1* and *SUMO2* mRNA expression correlate with *MYC* expression across the depicted conventional human PDAC cell lines. Pearson R and p values are indicated. n=2; all biological replicates were performed as technical duplicates. (B, C) MYC protein expression quantification by Western blot in human PDAC cell lines. Actin: loading control. (B) Representative MYC Western blot; (C) Quantification of the MYC Western blots. Protein expression of MYC in DanG cells was arbitrarily set to 1. Each dot represents a biological replicate. HPAF-II cells are not included in the representative Western blot of (B). Shown is the mean±SD. (D) representative Western blots of SUMO1 and SUMO2/3 in human PDAC cell lines. Actin: loading control. (E) MYC Western blot of IMIM-PC1^{MYC-ER} and IMIM-PC1 cells. Actin: loading control. (F) qPCR of *MYC*, *ODC1* and *CAD* in IMIM-PC1^{MYC-ER} cells. MYC downstream effectors *ODC1* and *CAD* are induced 24 hours after the treatment of IMIM-PC1 with 4-OHT at 500 nM. n=3; all biological replicates were performed as technical duplicates. P value of a paired t-test.(G, H) GSEA of RNA-Seq data of IMIM-PC1^{MYC-ER} treated for 24 hours with 4-OHT compared with vehicle controls. (I–M) The murine PDAC cell lines PPT-53631 and PPT-5671 were transduced with a GFP or an MYC-IRES-GFP vector. (I) MYC and GFP Western blot in parental, GFP-transduced and MYC-IRES-GFP-transduced cells. GAPDH: loading control. (J) Quantification of MYC expression corresponding to (I). Each circle represents quantification of a biological replicate. (K, L) GSEA of RNA-Seq data of GFP-transduced and MYC-IRES-GFP-transduced PPT-53631 cells. (M) Representative SUMO1 and SUMO2/3 Western blots of the indicated GFP-transduced and MYC-IRES-GFP-transduced cells; tubulin: loading control. (N) RNA-seq data of GFP-transduced and MYC-IRES-GFP-transduced PPT-53631 cells were analysed for the expression of Myc target genes and core SUMO pathway genes. Shown is the colour-coded log FC (fold change). mRNAs upregulated with an adjusted p<0.05 are marked by *. *P<0.05, **P<0.01. FDR, false discovery rate q value (GSE119423); 4-OHT, 4-hydroxytamoxifen; GSEA, gene set enrichment analysis; NES, Normalised Enrichment Score; PDAC, pancreatic ductal adenocarcinoma; SUMO, small ubiquitin-like modifier.

(figure 3N). Whether upregulation by MYC occurs directly or indirectly, is unclear and may vary with context. Together, across PDAC models and species, a functional connection of MYC to the SUMOylation machinery was observed, which supports the hypothesis of a specific vulnerability for inhibition of the SUMOylation pathway in MYC hyperactivated PDACs.

SUMO pathway inhibition induces G2/M phase arrest and apoptosis

To investigate whether the SUMOylation machinery is a relevant therapeutic target, we tested the activity of two small-molecule inhibitors of SAE. The selective SAE inhibitor ML-792 was demonstrated to inhibit SAE and SUMO-pathway activities.[35]

In breast, lung and colon cancer lines, ML-792 acts in an half-maximal effective concentration (EC_{50}) range of 60–450 nM to inhibit cell viability.[35] The dose–response curves measured with an MTT-viability assay of ML-792 in six human PDAC cell lines are shown in online supplementary figure S3A. The ML-792 half-maximal growth inhibitory (GI_{50}) concentrations in the PDAC lines are higher than the ones described in breast, lung and colon cancer lines[35] (online supplementary figure S3A). ML-93 is also a potent inhibitor of SAE, as measured in the ATP-inorganic pyrophosphate exchange assay, with a half-maximal inhibitory concentration of 37 nM when incubated with SUMO2, comparable to that reported for ML-792.[35] Assessment of cellular activity and selectivity of ML-93, measured by means of thioester assays, demonstrated potent inhibition of SAE with a EC_{50} value of 1 nM for inhibition of the UBC9-SUMO thioester, and dose-dependent decrease in global SUMOylation (online supplementary figure S3B). In contrast, EC_{50} values for inhibition of UBC12 and UBC10 thioesters by ML-93 were both >5000 nM, demonstrating strong selectivity of ML-93 for inhibition of the SUMO pathway relative to the NEDD8 and ubiquitin pathways.

ML-93 reduced growth (figure 4A) and clonogenic growth in the low nanomolar range (online supplementary figure S4A,B). In MiaPaCa2 and PSN1 cells, ML-93 increased the fraction of apoptotic cells in a dose-dependent and time-dependent manner (figure 4B). The apoptotic fraction is higher in *MYC*-amplified PSN1 cells. In MiaPaCa2 cells, ML-93 significantly reduced the fraction of cells in the G1 and S phases of the cell cycle with a distinct increase detected in the fraction of cells in the sub-G1 phase, demonstrating that apoptosis is a major contributor to the response (figure 4C). In addition, cells accumulated in the G2/M phase and we detected polyploidization on treatment with ML-93 (figure 4C). Loss of cells in the G1 phase of the cell cycle, polyploidization and induction of a sub-G1 population on treatment with ML-93 were also detected in PSN1 and PaTu-8988T cells (online supplementary figure S4C,D).

Pathways modulated on SUMOi and efficacy in MYC hyperactivated PDAC

To monitor inhibition of the pathway, we determined SUMOylation of the known SUMO substrate RanGAP1 in PaTu-8988T cells.[36] RanGAP1 is completely SUMOylated in PaTu-8988T cells and ML-93 induced the appearance of un-SUMOylated RanGAP1, demonstrating on-target activity (online supplementary figure S5A). RNA-seq of ML-93 treated PaTu-8988T cells showed that SUMOylation signatures were depleted (online supplementary figure S5B). To find pathways coinhibited by ML-93, we analysed RNA-seq data of three ML-93 treated human PDAC cell lines. Transcriptomic changes observed on ML-93 treatment were rather small and highly context dependent (online supplementary figure S5C). Also, pathways connected to ML-93-regulated genes varied with context (online supplementary figure S5D). Online supplementary figure S5E demonstrates MSigDB-derived hallmark signatures associated with ML-93 regulated genes, which were detected in all analysed cell lines. In addition to transcriptomics, we analysed ML-93-induced changes in protein expression on a global scale. Again, changes observed in the proteome analysis were rather moderate (online supplementary figure S5F).

To analyse the connection of SUMOi sensitivity to MYC activity, we used a large panel of human and murine PDAC cell lines. We determined GI_{50} values in 17 human conventional PDAC lines (figure 4D), and observed a distinct heterogeneity in the responsivity. Although MYC protein expression in whole cell lysates does not necessarily correlate with MYC's overall transcriptional activity, a consideration recently described in PDAC models,[21] human PDAC lines with higher MYC protein expression demonstrated activation of the MYC transcriptional network in GSEA (online supplementary figure S6A). These lines were characterised by significantly lower GI_{50} values (figure 4E). To validate our findings across different species, we used a $Kras^{G12D}$- and $PI3K/p110^{H1047R}$-driven murine PDAC cell line collection[37 38] and determined the GI_{50} values of ML-93 and ML-792 in 48 lines. GI_{50} values of ML-792 and ML-93 showed a significant correlation (figure 4F). We next investigated the connection of MYC with the sensitivity towards SUMOi at several levels. First, we analysed MYC protein expression in the most ML-93 sensitive (marked in blue in figure 4F) to the most resistant murine PDAC lines (marked in red in figure 4F). Murine ML-93 sensitive lines demonstrate higher MYC protein expression (figure 4G, H). In addition, we analysed RNA-seq data.[38] We defined murine PDAC lines which were sensitive or resistant to both SUMOi. Again, we observed an MYC signature in the sensitive cell lines (figure 4I). Third, we correlated the expression values of all transcripts of the murine expression dataset with the GI_{50} values for ML-792 and ML-93, determined Pearson correlation coefficients, and used these as a rank to run a preranked GSEA. Among the HALLMARK signatures associated with GI_{50} negatively correlated genes, both MYC HALLMARK signatures were detected (online supplementary figure S6B,C). Beyond demonstrating the correlation of MYC to SUMOi sensitivity, we used mechanistic data and models to functionalise the connection. We used the Project Score database (https://score.depmap.sanger.ac.uk/), which is based on a functional CRISPR/Cas drop-out screen.[39] The loss of fitness scores for MYC and UBE2I in 23 human PDAC cell lines were compared. A significant correlation of both scores was observed (figure 4J), supporting the notion, that MYC-addicted lines are coaddicted to the SUMO pathway. To further substantiate the finding that the SUMO pathway is an MYC-associated dependency, we used isogenic murine PDAC models. Such isogenic models are appropriate to find and define genotype-specific drug responses.[40] First, we used the MYC-IRES-GFP transduced cell lines PPT-53631 and PPT-5671 to perform a repopulation assay, allowing to monitor 'MYC-high' and 'MYC-low' population dynamics over time. Compared with GFP-transduced controls, MYC overexpressing cells showed a significant growth disadvantage under ML-93 treatment (figure 4K). Furthermore, a higher fraction of apoptotic cells was observed in MYC-transduced cells on SUMOi (figure 4L) and ML-93-dependent clonogenic growth inhibition was augmented by ectopic MYC expression (figure 4M). To further substantiate these findings, we used conditional MYC overexpression. First, murine PDAC lines were transduced with an MYC^{ER} coding vector (online supplementary figure S7A,B) and the response to ML-93 was measured in the presence (MYC on) or absence (MYC off) of 4-OHT. In all investigated models, the ML-93 dose response was shifted to the left in the presence of 4-OHT (online supplementary figure S7C), indicating a higher sensitivity. In PPT-53631 cells, mock transduced with the empty vector, 4-OHT does not change the ML-93 dose response, demonstrating a specific MYC effect (online supplementary figure S7C, far right panel). Also in clonogenic assays, the SUMOi response was augmented by activation of MYC (online supplementary figure S7D,E). To cross-species validate these findings, we used human IMIM-PC1^{MYCER} cells. Again, the dose response of both SUMOi was shifted to the left (online supplementary figure S7F), demonstrating that MYC hyperactivation generates a vulnerability which can be exploited

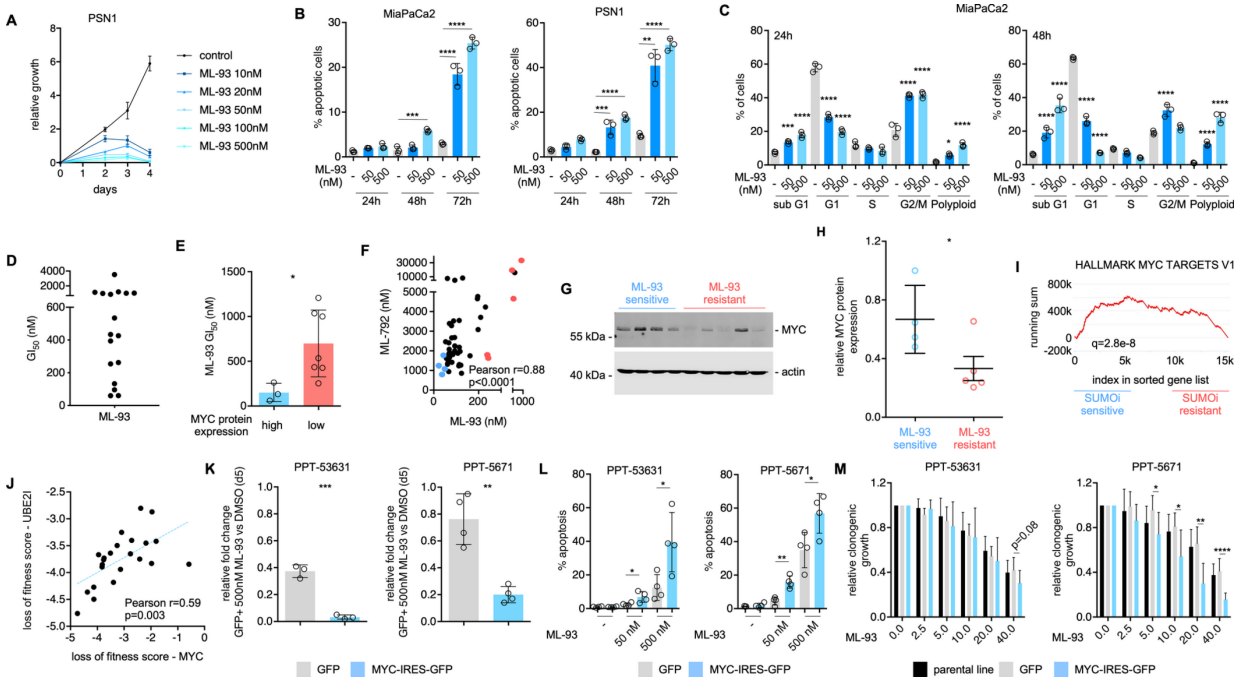

Figure 4 SUMOylation inhibition targets an MYC-associated vulnerability.(A) Growth kinetics reveal dose-dependent and time-dependent reduction of cell growth under ML-93 treatment. PSN1 cells were treated with varying concentrations of ML-93 for the indicated time points. Viable cells, determined by trypan blue exclusion, were determined at the indicated time points and relative growth is depicted. All replicates (n=3) were performed as technical triplicates. (B) ML-93 induces apoptosis as measured by annexin V/PI flow cytometric analysis at low nanomolar concentrations after treatment periods of 24 hours, 48 hours and 72 hours. All replicates (n=3) were performed as technical triplicates. ANOVA. **p<0.01, ***p<0.001, ****p<0.0001. (C) ML-93 induces G2/M cell cycle arrest as demonstrated by PI cell cycle flow cytometry analyses. Shown are the proportions of cells in the sub-G1, G1, S and G2/M phases after ML-93 treatment for 24 hours and 48 hours. All replicates (n=3) were performed as technical triplicates. ANOVA: **p<0.01, ***p<0.001, ****p<0.0001. (D) The growth inhibitory concentration 50% (GI_{50}) was determined in 17 human PDAC cell lines. ATP (CellTiter-Glo assay) was used as a surrogate to determine the dose response of a 7-point ML-93 dilution (0–1000 nM). Cells were treated for 72 hours. The assay was performed with at least three biological replicates conducted as technical triplicates. GI_{50} values >1000 nM were extrapolated from the fitted curve. (E) GI_{50} values of human PDAC lines with low and high MYC protein expression were compared. High expression: MYC protein expression >66th percentile; low expression: MYC protein expression <66th percentile (see figure 3C). *P value of an unpaired t-test <0.05. (F) GI_{50} for ML-93 and ML-792 was determined in 48 murine PDAC cell lines by MTT-assay. Determined was a dose response of 7-point dilution (ML-93: 0–1000 nM; ML-792: 0–5000 nM). Cells were treated for 72 hours. The assay was performed with at least three biological replicates conducted as technical triplicates. GI_{50} values >1000 nM for ML-93 and >5000 nM for ML-792 were extrapolated from the fitted curve. The Pearson correlation coefficient of ML-93 and ML-792 and the p values are depicted. Blue dots: ML-93 sensitive lines; red dots: ML-93 resistant lines. (G) MYC Western blot of the ML-93 sensitive and the ML-93 resistant murine PDAC cell lines. Actin: loading control. (H) Quantification of MYC expression in ML-93 sensitive and the ML-93-resistant murine PDAC cell lines, corresponding to (G). Mean MYC expression of three different lysates for each line, each normalised to actin. *P value of an unpaired t-test <0.05. (I) Unweighted GSEA analysis using the GeneTrail2 platform of SUMO inhibitor sensitive and resistant murine PDAC cell lines. Sensitive lines: common lines for which the ML-93 and the ML-792 GI_{50} values were <25th percentile. Resistant lines: common lines for which the ML-93 and the ML-792 GI_{50} values were >75th percentile. Q-value is depicted. (J) Loss of fitness scores were derived from the project score database (https://score.depmap.sanger.ac.uk/). Shown is the correlation of the scores for MYC and UBE2I in 23 human PDAC cell lines. The Pearson correlation coefficient and the p value are depicted. (K) Competitive repopulation assay. PPT-53631 and PPT-5671 cells transduced with a GFP or MYC-IRES-GFP vector were cocultured with corresponding wild type cells in a 20:80 ratio on D0. The proportion of GFP positive cells was tracked and reassessed on D5 by flow cytometry. The relative fold change was measured as the relative difference in the fraction of GFP positive cells on D5 versus baseline (d0). ML-93 (500 nM) treatment groups were normalised to the corresponding dimethylsulfoxide (DMSO)-treated controls and are depicted relative to all measured cells. All biological replicates (PPT-53631: n=3; PPT-5671: n=4) were performed as technical duplicates. P value of an unpaired t-test **<0.01, **<0.001. (L) Murine PPT-53631 or PPT-5671 PDAC cells, transduced with GFP or MYC-IRES-GFP vectors were treated with 50, and 500 nM ML-93 for 72 hours. The fraction of apoptotic cells was determined by annexin V/DAPI flow cytometric analysis. All annexin V positive and DAPI negative cells were rated as apoptotic. Four independent experiments are shown and each experiment is depicted as a circle. P value of an unpaired t-test **<0.01; *<0.05. (M) Quantification of clonogenic assays in parental, GFP or MYC-IRES-GFP vector transduced murine PPT-53631 and PPT-5671 PDAC cell lines. Cells were treated with the indicated ML-93 doses. Assay was performed with at least three biological replicates in technical duplicates. P value of an unpaired t-test: *<0.05, **<0.01, ****<0.0001. ANOVA, analysis of variance; GSEA, gene set enrichment analysis; PDAC, pancreatic ductal adenocarcinoma; SUMO, small ubiquitin-like modifier.

through SUMOi. To extend this note to the genetic level, we used *Ube2i* RNA interference in MYC overexpressing models. However, due to a distinct counterselection, we were not able to achieve a meaningful knock-down. In an assumption that SUMOi resistant cells will better tolerate the *Ube2i* knock-down, we transduced such a cell line with an MYC^{ER} vector (online supplementary figure S7G,A). However, also here, only one of the tested shRNAs induced a *Ube2i* knockdown to approximately 50% compared with control (online supplementary figure S7H). Despite this modest knock-down, activation of MYC by

4-OHT is less tolerated in *Ube2i*-depleted cells, underscoring the connection of both pathways (online supplementary figure S7I).

SUMOi sensitivity in human PDAC ex vivo and in vivo models

To elucidate first evidence for in vivo activity of ML-93, we used xenograft transplantation models. First, we determined in vivo toxicity of ML-93 in C57BL/6 mice (online supplementary figure S8A). No significant change in body weight (online supplementary figure S8B), haemoglobin concentration, white blood cells or platelets counts were detected (online supplementary figure S8C). SUMO2/3 western blots of splenocyte protein lysates demonstrated on-target activity (online supplementary figure S8D,E). Of note, only in immunodeficient mice, we observed ML-93-induced skin irritation and ulceration at the injection site. To investigate activity of ML-93 against PDAC in vivo, we transplanted PaTu-8988T cells s.c. into immunocompromised NOG mice and treated tumor-bearing mice with ML-93 (figure 5A). Growth of PaTu-8988T xenografts was inhibited by ML-93 (figure 5B,C). To monitor inhibition of the pathway in vivo, we determined again SUMOylation of RanGAP1[36] (figure 5D) and observed reduced SUMOylation of RanGAP1 (figure 5E). In addition to PaTu-8988T, we tested ML-93 in PSN1, HuPDAC7, BxPc3 and IMIM-PC1 in vivo models (online supplementary figure S8F-J). Although the proliferation index was reduced by ML-93 in the PSN1 in vivo model, tumour growth was not altered in any of the investigated models in the limited-duration treatment schedule used.

To investigate the connection of MYC with the sensitivity towards SUMOi in primary human ex vivo models, we used patient-derived organoids (PDOs) and primary-dispersed human PDAC cell lines. PDOs are 3D models suitable to evaluate clinically relevant therapeutic vulnerabilities.[41–43] Consistent with the two-dimensional cultures, ML-93 was found to inhibit viability in the double-digit nanomolar range in three out of four of the investigated PDO models, whereas one PDO completely resisted ML-93 treatment (online supplementary figure S9A). Although the moderate number of organoids analysed clearly limits the informative value, the resistant PDO showed the lowest *MYC* mRNA expression (online supplementary figure S9B). Such observations underscore the requirement to stratify patients for SUMO pathway targeting drugs. Complementary to PDO models, we used primary-dispersed human PDAC cell lines. We first analysed the MYC expression and SUMO status in three lines and observed a gradual increase in MYC protein expression from HuPDAC3, to HuPDAC17 and HuPDAC7 (figure 5F and online supplementary figure S9C). Gradual increase in MYC expression is correlated to an increase in SUMO1 and SUMO2/3 modified proteins (figure 5G). MYC target genes and SUMO-pathway genes showed lower expression at the mRNA level in HuPDAC3 cells (figure 5H), demonstrating that the MYC/SUMO 'high' subtype we described in PDAC, was recapitulated by the primary-dispersed human PDAC cell lines. Importantly, the MYC/SUMO expression status is connected to the sensitivity towards SUMOi as demonstrated by different GI_{50} values and inhibition of clonogenic growth (figure 5I–K; online supplementary figure S9D). Consistently, the fraction of apoptotic cells was higher in HuPDAC7 cells on SUMOi compared with the line with low MYC expression (figure 5L).

DISCUSSION

The ability to target molecularly defined tumour subtype-specific drivers is a successful strategy and has changed the standard of care in solid tumour entities. Although the existence of different subtypes in PDAC is undisputed, therapeutically exploitable subtype-specific drivers and resulting dependencies were so far unknown for the majority of patients. In this study, we provide for the first-time evidence for the existence of a PDAC subtype characterised by the coactivation of the MYC and SUMO pathways and connected to a worse prognosis. We detected an enrichment of tumours coactivating MYC and SUMO in the basal-like/squamous subtype of the disease, a subtype especially resistant to chemotherapies.[15 16] We show a mechanistic relationship of the *MYC* oncogene to the SUMOylation machinery in PDAC and provide evidence that MYC hyperactivation increases the sensitivity to SUMO pathway inhibition.

One strategy to target MYC is to identify synthetic dosage lethal interactions associated with hyperactivity of this transcription factor.[17 18 20] The utility of such a concept is underscored by the results of a genome-wide shRNA MYC synthetic lethality screen in HMECs, where SUMOylation pathway members, including *SAE2/UBA2*, *SAE1* or *UBE2I*, were defined as synthetic lethal MYC interactions.[28] Additionally, *UBE2I* was detected in an MYC synthetic lethal screen in human foreskin fibroblasts,[44] demonstrating the robust synthetic lethal relationship of MYC and the SUMO pathway. Genetic interference with the SUMOylation pathway in the MYC hyperactive state induced an accumulation of the cells in the G2/M-phase of the cell cycle, polyploidization and subsequent apoptosis.[28 29] At the pharmacological level, the selective SAE inhibitor ML-792 phenocopies the genetic inhibition of the SUMOylation pathway and acts preferentially in MYC hyperactive states.[35] Consistent with the above-mentioned data, we detected that ML-93, which shows a higher efficacy in cell-based PDAC models, acts in the nanomolar range, induced accumulation of cells in the G2/M phase, polyploidy and apoptosis. Furthermore, we provide multiple evidences for a preferential efficacy of ML-93 in MYC-hyperactivated PDACs. It has been described that MYC primes for sensitivity towards antimitotic drugs acting in the G2/M phase of the cell cycle,[45] especially in the context of mutant KRAS,[46] a ubiquitous genetic lesion in PDAC. In addition, genes relevant for mitotic control are enriched among MYC synthetic lethal genes,[28 44] furthermore supporting the observation that MYC hyperactivation induces a vulnerability in this particular cell cycle phase. Congruently, the SUMO pathway is necessary for cell division and regulates mitotic chromosome structure, kinetochores, mitotic progression, chromosome separation and cytokinesis,[47] explaining the synthetic lethal interaction of the SUMO pathway with MYC.

Although we detected a coexpression of MYC and SUMO in a PDAC subtype, it is important to note that especially in the IHC analysis there was evidence for an active SUMO pathway, measured as nuclear expression of SUMO1, that was also detected in PDAC with low MYC expression. The molecular drivers in this setting remain elusive so far. Vice versa, MYC positive PDAC with no activation of the SUMO pathway do also exist. In breast cancers, the SUMO pathway enzymes SAE1 and SAE2 mark a patient population with particular worse prognosis only in the MYC high subtype,[28] an effect we did not observe in PDAC using SUMO proteins as discriminators. Such observations point to the complexity and context specific regulation of the MYC network. Here, MYC cofactors can add to the complexity and the understanding of the network. For example, the ATP-dependent nucleosome-remodelling factor component bromodomain PHD transcription factor BPTF was demonstrated to be necessary for the control of an MYC subnetwork in pancreatic cancer.[48] Such considerations might also implicate that the association of hyperactive MYC to one particular transcriptome-defined PDAC

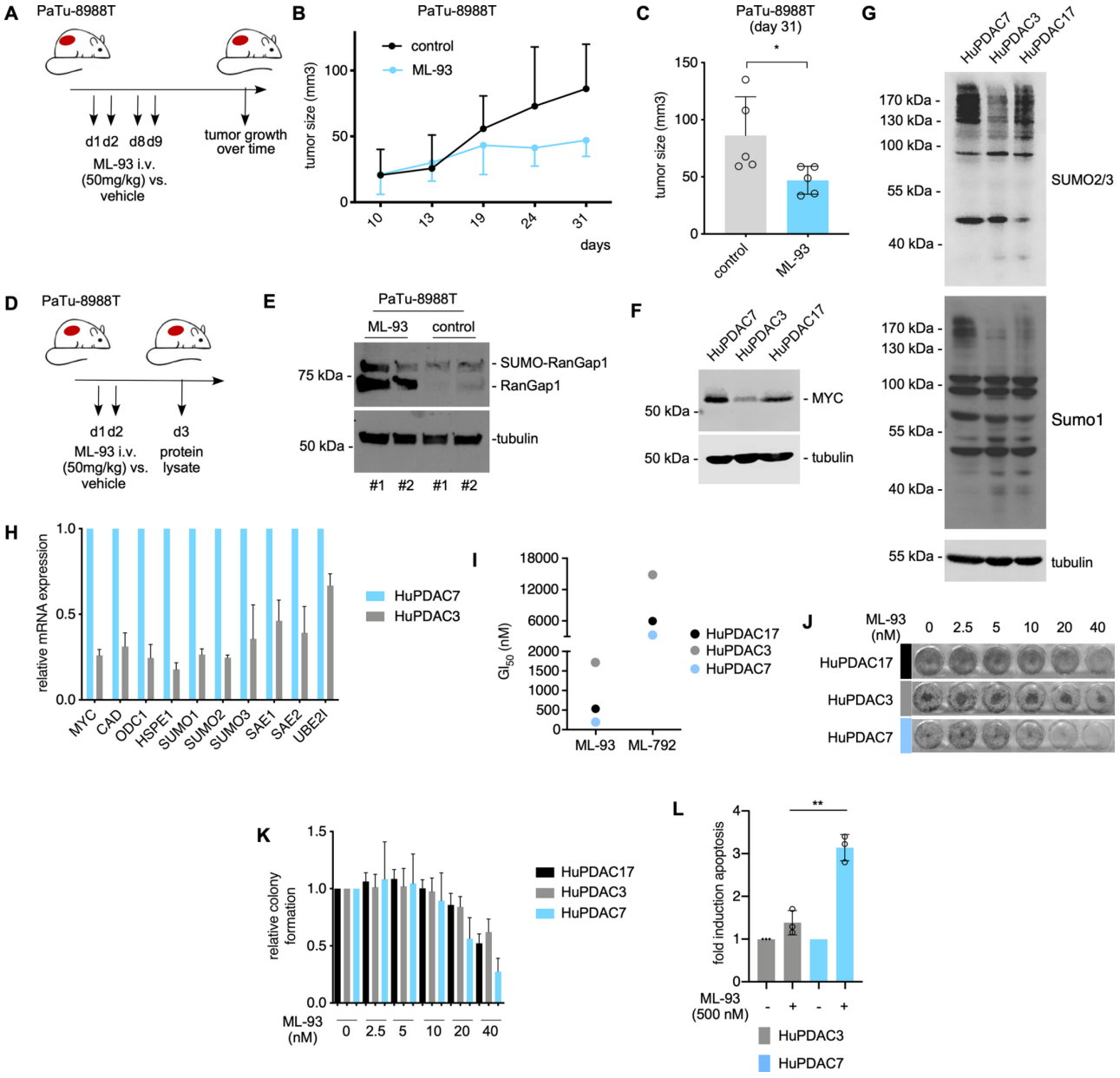

Figure 5 SUMOylation inhibition in human PDAC ex vivo and in vivo models. (A–E) The human PDAC cell line PaTu-8988T was used to generate murine xenograft models in NOG mice. (A) Mice were treated with 50 mg/kg ML-93 intravenously on d1,2 and d8,9 and (B) tumour size was measured over time. (C) Tumour size at D31 of ML-93-treated PaTu-8988T-derived xenograft mice revealed significant reduction in tumour size in treated mice (n=5 mice in each group). Statistical significance was assessed using an unpaired Student's t-test. *P<0.05. PaTu-8988T tumours were treated with 50 mg/kg ML-93 intravenously on D1, 2 (D). Two days after the first injection (d3), tumours were harvested and proteins were analysed for sumoylated and un-SUMOylated RanGAP1 by Western blot (E). Tumour lysates of two vehicle-treated and two ML-93-treated animals were analysed tubulin: loading control. (F) Primary-dispersed human PDAC cells, HuPDAC3, HuPDAC7, HuPDAC17, were analysed for MYC expression by Western blotting; tubulin: loading control. (G) SUMO1 and SUMO2/3 Western blots of the indicated cell lines; tubulin: loading control. (H) Primary-dispersed human PDAC cells, HuPDAC3 and HuPDAC7 were analysed for the mRNA expression of *MYC*, *CAD*, *ODC1*, *HSPE1* (MYC pathway) and *SUMO1*, *SUMO2*, *SUMO3*, *SAE1*, *SAE2*, *UBE2I* (SUMO pathway). mRNA expression was normalised to *GAPDH* and the mRNA expression in HuPDAC7 was arbitrarily set to 1. Shown is the mean±SD of three independent experiments performed as technical triplicates. (I) GI_{50} for ML-93 and ML-792 was determined in HuPDAC3, HuPDAC7, HuPDAC17 cells using CellTiter-Glo assay. A 7-point dilution (ML-93: 0–1000 nM; ML-792: 0–5000 nM) was used and cells were treated for 72 hours. The assay was performed with at least three biological replicates conducted as technical triplicates. GI_{50} values >1000 nM for ML-93 and >5000 nM for ML-792 were extrapolated from the fitted curve. (J, K) Clonogenic assay of HuPDAC3, HuPDAC7, HuPDAC17 cells treated with the indicated doses of ML-93 or vehicle. (E) Representative experiment is depicted; (F) Quantification of the clonogenic assay. Shown is the mean±SD of at least three biological replicates performed as duplicates. (L) Human HuPDAC3 and HuPDAC7 cells were treated with ML-93 (500 nM) or were left as vehicle treated controls. After 72 hours, the fraction of apoptotic cells was determined by annexin V/PI flow cytometric analysis. All annexin V positive and PI negative cells were rated as apoptotic. Shown is the fold induction determined as the relative increase in the apoptotic fraction versus DMSO control after 72 hours of treatment with ML-93. Three independent experiments performed as technical triplicates are shown and each experiment is depicted as a circle. P value of an unpaired t-test *<0.05; **<0.01. GI_{50}, growth inhibitory; i.v., intravenous; PDAC, pancreatic ductal adenocarcinoma; SUMO, small ubiquitin-like modifier.

subtype is less strict than anticipated and the net MYC activity is modulated by coexpression of cofactors and synthetically lethal interactors, a note recently described across human cancers.[49] The demonstration that MYC is central to plasticity processes in PDAC models,[50] might furthermore underscore the need for MYC in diverse cellular states and phenotypes.

Despite multiple evidence for the synthetic lethal interaction of MYC and SUMO pathways, only one out of three MYC 'high' models responded to SUMOi in vivo. This phenomenon might be explained at several levels. Clear evidence, including the recent VIKTORY umbrella trial in gastric cancer,[51] demonstrates that biomarker-driven patient selection to targeted therapies is successful. However, despite the presence of the marker, only a fraction of patients responds to the targeted intervention. This implicates that the biology associated with a particular marker must be analysed and understood in greater and mechanistic detail. Furthermore, two or more markers might increase the precision to select therapies in solid cancers, a note underscored by large cell-based screening efforts.[52] The observation that PSN1 cells react in vivo with a trend for reduced proliferation and increased caspase activity shortly after the SUMOi application, but SUMOi does not reduce tumour burden, might suggest that alternative treatment schedules should be tested to increase the efficacy of the treatment. Slow growth and small size of the investigated in vivo models might also impact on the efficacy. Furthermore, due to the ML-93-induced skin irritation and ulceration at the injection site observed in immunodeficient mice, we were not able to investigate extended treatment regimens. Other explanations include problems of bioavailability of drugs and resistance mechanisms that are initiated in vivo. Several promising anticancer drugs, such as proteasome inhibitors, HDAC inhibitors, heat-shock protein inhibitors and mitotic inhibitors, are potent in vitro but exhibit limited efficacy in solid cancers models in vivo. Reduced oxygen tension, metabolic supply, translation rate (and hence proteotoxic stress) and rate of proliferation of cell lines growing in vivo can be attributed to explain the discrepancy.[53–56] Lastly, dual or triple combinations of targeted therapies are successfully used in the clinic. For BRAF-mutated melanomas, dual targeting of the driver pathway with an RAF and an MEK-inhibitor is FDA approved.[57] In a recent safety lead-in analysis of the BEACON phase III clinical trial for BRAF mutant colorectal cancer promising efficacy of a triple targeted therapy with raf proto-oncogene, serine/threonine kinase (RAF), mitogen-activated protein kinase kinase (MEK) and epidermal growth factor receptor (EGFR)-inhibitors was observed.[58] Such data suggest to develop SUMOi-based combination therapies by an unbiased pharmacological screening experiment to exploit MYC synthetic dosage lethality by a multiple-targeting approach.

We provide clear rationale for the future development of SUMOylation inhibitor-based therapies for a PDAC subgroup with coactivation of the SUMO pathway and MYC. This particular PDAC population is characterised by an aggressive disease, poor prognosis and the current lack of clear treatment options. Therefore, our study represents an important step in establishing SUMOi-based therapy as a potential approach to target an extremely dismal PDAC subtype.

Author affiliations
[1]Medical Clinic and Policlinic III, Klinikum rechts der Isar, Technical University Munich, München, Germany
[2]Medical Clinic and Polyclinic II, Klinikum rechts der Isar, Technical University Munich, München, Germany
[3]Department of Hematology, Oncology and Tumor Immunology, Campus Benjamin Franklin, Charité - Universitätsmedizin Berlin, Berlin, Germany
[4]Center for Bioinformatics, Saarland Informatics Campus, Saarland University, Saarbrücken, Germany
[5]Saarbrücken Graduate School of Computer Science, Saarland Informatics Campus, Saarland University, Saarbrücken, Germany
[6]Institute of Pathology, Technical University Munich, München, Germany
[7]Department of Surgery, Sahlgrenska Cancer Center, Gothenburg University, Gothenburg, Sweden
[8]German Cancer Research Center (DKFZ) and German Cancer Consortium (DKTK), Heidelberg, Germany
[9]Goethe University, Medical School, Institute of Biochemistry II, Frankfurt, Germany
[10]Oncology Drug Discovery Unit, Takeda Pharmaceuticals International Co, Cambridge, Massachusetts, USA
[11]Institute for Translational Cancer Research and Experimental Cancer Therapy, Technical University Munich, München, Germany
[12]Institute of Molecular Oncology and Functional Genomics, Technical University Munich, München, Germany

Acknowledgements ML-792 and ML-93 was provided by Millennium Pharmaceuticals, a wholly owned subsidiary of Takeda Pharmaceutical Company. We thank Jessica Riceberg for contributing to this work by generating the thioester western blot, Sofia Stenqvist for excellent assistance for the in vivo experiments and Denis Huszar (Takeda) for critical reading the manuscript. Part of the results shown here is based on data generated by the TCGA Research Network: https://cancergenome.nih.gov.

Contributors Conception and design of the study: AB, ZH, MS, CS, MW, GS and UK. Acquisition of data and/or analysis and interpretation of data: AB, ZH, LS, MS, YH, GS, JS, AS, LN, WW, ZD, CS, KS, LS, H-PL, AC, FO, JS, KS, DS, MS, RR, WW, JN, MR, GS and UK; Drafting of the manuscript: AB, ZH, CS, MS, GS and UK. All authors revised the manuscript for important intellectual content and approved the final version submitted for publication.

Funding This work was supported by the Wilhelm-Sander Foundation (2017.048.1 to UK and GS), Deutsche Forschungsgemeinschaft (DFG) (SFB824/C3 and SFB1335/P3 to UK, SFB824/C9 to GS and DS, SFB1321/S01 to WW, KS, MR, DS, RR, GS and SCHN959/3-1 to GS), Deutsche Krebshilfe (111273 (Max-Eder Program) to MR, 111944 to UK), Else-Kröner-Fresenius-Stiftung (2016_A43 to MW), Stiftung Charité (to UK) and DKTK Joint Funding to RR, WW, DS and GS).

Competing interests SL is an employee of Takeda Pharmaceutical Company.

Patient consent for publication Not required.

Ethics approval The primary human PDAC models were established and analysed in accordance with the Declaration of Helsinki and were approved by the local ethical committee (Project 207/15, 1946/07 and 330/19).

Provenance and peer review Not commissioned; externally peer reviewed.

Data availability statement Data are available in a public, open access repository. Transcriptomic Data, NCBI Geo, freely available: GSE119423 / PRJNA489233 https://www.ncbi.nlm.nih.gov/geo/query/acc.cgi?acc=GSE119423 Transcriptomic Data, ENA, freely available: PRJEB34637 https://www.ebi.ac.uk/ena/data/view/PRJEB34637Proteome Data, ProteomeXchange, PRIDE database, freely available:PXD011347 http://www.ebi.ac.uk/pride/archive/projects/PXD011347.

ORCID iDs
Zonera Hassan http://orcid.org/0000-0002-8485-1958
Maximilian Reichert http://orcid.org/0000-0002-8611-5639
Günter Schneider http://orcid.org/0000-0003-1840-4508
Ulrich Keller https://orcid.org/0000-0002-8485-1958

REFERENCES

1 Siegel RL, Miller KD, Jemal A, *et al*. Cancer statistics, 2019. *CA A Cancer J Clin* 2019;69:7–34.
2 Notta F, Hahn SA, Real FX. A genetic roadmap of pancreatic cancer: still evolving. *Gut* 2017;66:2170–8.
3 Kleeff J, Korc M, Apte M, *et al*. Pancreatic cancer. *Nat Rev Dis Primers* 2016;2:16022.
4 Golan T, Hammel P, Reni M, *et al*. Maintenance Olaparib for Germline *BRCA* -Mutated Metastatic Pancreatic Cancer. *N Engl J Med* 2019;381:317–27.
5 Nicolle R, Blum Y, Marisa L, *et al*. Pancreatic adenocarcinoma therapeutic targets revealed by tumor-stroma cross-talk analyses in patient-derived xenografts. *Cell Rep* 2017;21:2458–70.

6 Cancer Genome Atlas Research Network. Electronic address aadhe, cancer genome atlas research N. integrated genomic characterization of pancreatic ductal adenocarcinoma. *Cancer Cell* 2017;32:185–203.
7 Bailey P, Chang DK, Nones K, *et al*. Genomic analyses identify molecular subtypes of pancreatic cancer. *Nature* 2016;531:47–52.
8 Collisson EA, Sadanandam A, Olson P, *et al*. Subtypes of pancreatic ductal adenocarcinoma and their differing responses to therapy. *Nat Med* 2011;17:500–3.
9 Daemen A, Peterson D, Sahu N, *et al*. Metabolite profiling stratifies pancreatic ductal adenocarcinomas into subtypes with distinct sensitivities to metabolic inhibitors. *Proc Natl Acad Sci U S A* 2015;112:E4410–7.
10 Moffitt RA, Marayati R, Flate EL, *et al*. Virtual microdissection identifies distinct tumor- and stroma-specific subtypes of pancreatic ductal adenocarcinoma. *Nat Genet* 2015;47:1168–78.
11 Lomberk G, Blum Y, Nicolle R, *et al*. Distinct epigenetic landscapes underlie the pathobiology of pancreatic cancer subtypes. *Nat Commun* 1978;2018:9.
12 Noll EM, Eisen C, Stenzinger A, *et al*. Cyp3A5 mediates basal and acquired therapy resistance in different subtypes of pancreatic ductal adenocarcinoma. *Nat Med* 2016;22:278–87.
13 Waddell N, Pajic M, Patch A-M, *et al*. Whole genomes redefine the mutational landscape of pancreatic cancer. *Nature* 2015;518:495–501.
14 Karasinska JM, Topham JT, Kalloger SE, *et al*. Altered gene expression along the Glycolysis-Cholesterol synthesis axis is associated with outcome in pancreatic cancer. *Clin Cancer Res* 2020;26:1–6.
15 Muckenhuber A, Berger AK, Schlitter AM, *et al*. Pancreatic ductal adenocarcinoma subtyping using the biomarkers hepatocyte nuclear factor-1A and Cytokeratin-81 correlates with outcome and treatment response. *Clin Cancer Res* 2018;24:351–9.
16 Aung KL, Fischer SE, Denroche RE, *et al*. Genomics-Driven precision medicine for advanced pancreatic cancer: early results from the COMPASS trial. *Clin Cancer Res* 2018;24:1344–54.
17 Wirth M, Mahboobi S, Kra mer OH, *et al*. Concepts to target Myc in pancreatic cancer. *Mol Cancer Ther* 2016;15:1792–8.
18 Wirth M, Schneider G. Myc: a stratification marker for pancreatic cancer therapy. *Trends in Cancer* 2016;2:1–3.
19 Hessmann E, Schneider G, Ellenrieder V, *et al*. Myc in pancreatic cancer: novel mechanistic insights and their translation into therapeutic strategies. *Oncogene* 2016;35:1609–18.
20 Cermelli S, Jang IS, Bernard B, *et al*. Synthetic lethal screens as a means to understand and treat Myc-driven cancers. *Cold Spring Harb Perspect Med* 2014;4:a014209.
21 Bian B, Bigonnet M, Gayet O, *et al*. Gene expression profiling of patient-derived pancreatic cancer xenografts predicts sensitivity to the BET bromodomain inhibitor JQ1: implications for individualized medicine efforts. *EMBO Mol Med* 2017;9:482–97.
22 Bian B, Juiz NA, Gayet O, *et al*. Pancreatic cancer organoids for determining sensitivity to bromodomain and extra-terminal inhibitors (BETi). *Front Oncol* 2019;9:475.
23 Boj SF, Hwang C-I, Baker LA, *et al*. Organoid models of human and mouse ductal pancreatic cancer. *Cell* 2015;160:324–38.
24 Hassan Z, Schneeweis C, Wirth M, *et al*. Mtor inhibitor-based combination therapies for pancreatic cancer. *Br J Cancer* 2018;118:366–77.
25 Conradt L, Godl K, Schaab C, *et al*. Disclosure of erlotinib as a multikinase inhibitor in pancreatic ductal adenocarcinoma. *Neoplasia* 2011;13:1026–34.
26 Witkiewicz AK, McMillan EA, Balaji U, *et al*. Whole-Exome sequencing of pancreatic cancer defines genetic diversity and therapeutic targets. *Nat Commun* 2015;6:6744.
27 Stöckel D, Kehl T, Trampert P, *et al*. Multi-Omics enrichment analysis using the GeneTrail2 web service. *Bioinformatics* 2016;32:1502–8.
28 Kessler JD, Kahle KT, Sun T, *et al*. A SUMOylation-dependent transcriptional subprogram is required for Myc-driven tumorigenesis. *Science* 2012;335:348–53.
29 Hoellein A, Fallahi M, Schoeffmann S, *et al*. Myc-Induced sumoylation is a therapeutic vulnerability for B-cell lymphoma. *Blood* 2014;124:2081–90.
30 Seeler J-S, Dejean A. Sumo and the robustness of cancer. *Nat Rev Cancer* 2017;17:184–97.
31 Flotho A, Melchior F. Sumoylation: a regulatory protein modification in health and disease. *Annu Rev Biochem* 2013;82:357–85.
32 Yang S, He P, Wang J, *et al*. A novel MIF signaling pathway drives the malignant character of pancreatic cancer by targeting NR3C2. *Cancer Res* 2016;76:3838–50.
33 Collisson EA, Bailey P, Chang DK, *et al*. Molecular subtypes of pancreatic cancer. *Nat Rev Gastroenterol Hepatol* 2019;16:207–20.
34 Jung LA, Gebhardt A, Koelmel W, *et al*. OmoMYC blunts promoter invasion by oncogenic Myc to inhibit gene expression characteristic of Myc-dependent tumors. *Oncogene* 2017;36:1911–24.
35 He X, Riceberg J, Soucy T, *et al*. Probing the roles of sumoylation in cancer cell biology by using a selective SAE inhibitor. *Nat Chem Biol* 2017;13:1164–71.
36 Bernier-Villamor V, Sampson DA, Matunis MJ, *et al*. Structural basis for E2-mediated SUMO conjugation revealed by a complex between ubiquitin-conjugating enzyme Ubc9 and RanGAP1. *Cell* 2002;108:345–56.
37 Eser S, Reiff N, Messer M, *et al*. Selective requirement of PI3K/PDK1 signaling for KRAS oncogene-driven pancreatic cell plasticity and cancer. *Cancer Cell* 2013;23:406–20.
38 Mueller S, Engleitner T, Maresch R, *et al*. Evolutionary routes and KRAS dosage define pancreatic cancer phenotypes. *Nature* 2018;554:62–8.
39 Behan FM, Iorio F, Picco G, *et al*. Prioritization of cancer therapeutic targets using CRISPR–Cas9 screens. *Nature* 2019;568:511–6.
40 Martins MM, Zhou AY, Corella A, *et al*. Linking tumor mutations to drug responses via a quantitative chemical-genetic interaction map. *Cancer Discov* 2015;5:154–67.
41 Vlachogiannis G, Hedayat S, Vatsiou A, *et al*. Patient-Derived organoids model treatment response of metastatic gastrointestinal cancers. *Science* 2018;359:920–6.
42 Pauli C, Hopkins BD, Prandi D, *et al*. Personalized *In Vitro* and *In Vivo* Cancer Models to Guide Precision Medicine. *Cancer Discov* 2017;7:462–77.
43 Tiriac H, Belleau P, Engle DD, *et al*. Organoid profiling identifies common responders to chemotherapy in pancreatic cancer. *Cancer Discov* 2018;8:1112–29.
44 Toyoshima M, Howie HL, Imakura M, *et al*. Functional genomics identifies therapeutic targets for Myc-driven cancer. *Proc Natl Acad Sci U S A* 2012;109:9545–50.
45 Topham C, Tighe A, Ly P, *et al*. Myc is a major determinant of mitotic cell fate. *Cancer Cell* 2015;28:129–40.
46 Perera D, Venkitaraman AR. Oncogenic KRAS triggers MAPK-dependent errors in mitosis and Myc-dependent sensitivity to anti-mitotic agents. *Sci Rep* 2016;6:29741.
47 Mukhopadhyay D, Dasso M. The SUMO pathway in mitosis. *Adv Exp Med Biol* 2017;963:171–84.
48 Richart L, Carrillo-de Santa Pau E, Río-Machín A, *et al*. Bptf is required for c-myc transcriptional activity and in vivo tumorigenesis. *Nat Commun* 2016;7:10153.
49 Magen A, Das Sahu A, Lee JS, *et al*. Beyond synthetic lethality: Charting the landscape of pairwise gene expression states associated with survival in cancer. *Cell Rep* 2019;28:938–48.
50 Farrell AS, Joly MM, Allen-Petersen BL, *et al*. Myc regulates ductal-neuroendocrine lineage plasticity in pancreatic ductal adenocarcinoma associated with poor outcome and chemoresistance. *Nat Commun* 1728;2017:8.
51 Lee J, Kim ST, Kim K, *et al*. Tumor genomic profiling guides metastatic gastric cancer patients to targeted treatment: the VIKTORY umbrella trial. *Cancer Discov* 2019;9:CD-19-0442–405.
52 Iorio F, Knijnenburg TA, Vis DJ, *et al*. A landscape of pharmacogenomic interactions in cancer. *Cell* 2016;166:740–54.
53 Rixe O, Fojo T. Is cell death a critical end point for anticancer therapies or is cytostasis sufficient? *Clin Cancer Res* 2007;13:7280–7.
54 Bhadury J, Einarsdottir BO, Podraza A, *et al*. Hypoxia-Regulated gene expression explains differences between melanoma cell line-derived xenografts and patient-derived xenografts. *Oncotarget* 2016;7:23801–11.
55 Gillet J-P, Calcagno AM, Varma S, *et al*. Redefining the relevance of established cancer cell lines to the study of mechanisms of clinical anti-cancer drug resistance. *Proc Natl Acad Sci U S A* 2011;108:18708–13.
56 Johnson JI, Decker S, Zaharevitz D, *et al*. Relationships between drug activity in NCI preclinical in vitro and in vivo models and early clinical trials. *Br J Cancer* 2001;84:1424–31.
57 Flaherty KT, Infante JR, Daud A, *et al*. Combined BRAF and MEK inhibition in melanoma with BRAF V600 mutations. *N Engl J Med* 2012;367:1694–703.
58 Van Cutsem E, Huijberts S, Grothey A, *et al*. Binimetinib, Encorafenib, and Cetuximab Triplet Therapy for Patients With *BRAF* V600E–Mutant Metastatic Colorectal Cancer: Safety Lead-In Results From the Phase III BEACON Colorectal Cancer Study. *JCO* 2019;37:1460–9.

SUPPLEMENTAL METHODS

Cell culture

MiaPaCa2 and PaTu-8988T cell lines were cultured in DMEM (Gibco/Life Technologies, Darmstadt, Germany) supplemented with 10% fetal calf serum (FCS) (Merck Millipore/Biochrom, Berlin, Germany). DanG, BxPc3, PSN1, IMIM-PC1, HUPT4, PaTu-8988S, ASPC1, SW1990, MZ1-PC, SU8686, PANC0203, PANC0504, HPAC, HUPT3 and HPAFII cells were cultured in RPMI 1640 medium (Gibco/Life Technologies™, Darmstadt, Germany) supplemented with 10% FCS. HCT116 cells were cultured in McCoy's 5A medium supplemented with 10% FCS. All cell culture media were supplemented with 1% (w/v) penicillin/streptomycin (ThermoFisherScientific/Life technologies, Waltham, MA, USA). Establishment of murine PDAC cell lines has been described previously [1]. The used lines were established from murine *Kras*^{G12D}-driven or *PI3K/p110*^{H1047R}-driven murine PDACs [2, 3]. Murine PDACs cell lines were cultured in DMEM medium (Gibco/Life Technologies) supplemented with 10% FCS and 1% (w/v) penicillin/streptomycin. Identity of the murine PDAC cell lines was verified using genotyping PCR. Human cell lines were authenticated by Single Nucleotide Polymorphism (SNP)-Profiling conducted by Multiplexion (Multiplexion GmbH, Heidelberg, Germany) or short tandem repeat (STR) profiling (Mycrosynth, Balgach, Switzerland). Cell lines were tested for Mycoplasma contamination by a PCR-based method [4] or externally tested by Multiplexion (Multiplexion GmbH, Heidelberg, Germany).

Generation of patient-derived PDAC organoids and primary-dispersed cell lines

Primary patient-derived PDAC 3D organoids were generated from primary resected human pancreatic adenocarcinoma surgical specimen according to the Tuveson protocol described in [5] and [6]. Diagnosis of PDAC was confirmed by pathological examination. The primary human PDAC 3D organoid models and primary-dispersed cell lines were established and analyzed in accordance with the declaration of Helsinki, were approved by the local ethical committee (Project 207/15, 1946/07, and 330/19), and written informed consent from the patients for research use was obtained prior to the investigation. All organoids used have a

documented *KRAS* mutation: B25: G12V, B48: G12D, B54: G12D, B61: G12D. Due to continuous experimentation with these lines and re-thaw failures, some of these lines are not available for further experimentation. For drug screening purposes, organoids were dispensed through enzymatic (TrypLE Reagents, Thermo Scientific) and mechanical force. Cell-Matrigel suspensions were placed into 96-well plates and ML-93 treatment was initiated 24 hours after plating. Viability of cultures was measured 5 days after drug addition via CellTiter-Glo 3D Cell Viability Assay (Promega, Mannheim, Germany) using a luminescence microplate reader (FLUOstar OPTIMA).

Primary-dispersed human PDAC cells (HuPDAC3, HuPDAC7, HuPDAC17) were isolated from surgically-resected (HuPDAC3, HuPDAC17) or PdX-derived (HuPDAC7) human PDAC as described [7]. These cells were cultured in RPMI 1640 Medium (Gibco/Life Technologies^{TM}, Darmstadt, Germany) supplemented with 20% FCS and 1% Penicillin-Streptomycin (Merck, Sigma-Aldrich, Darmstadt, Germany). The cells were used in-between passage 10-20 in all experiments. All primary-dispersed human PDAC cell lines harbor a *KRAS*^{G12D} mutation.

Retroviral transduction

Human PDAC cell line IMIM-PC1 was engineered to stably express the ecotropic receptor via transduction with MSCV-rtTA-IRES-EcoReceptor-PGK-puro followed by selection with puromycin as described [8]. The IMIM-PC1 RIEP cell line (expressing the ecotropic receptor) was infected to stably express the MYC-estrogen receptor (MYC^{ER}) fusion protein via retroviral transduction with the MSCV MYC^{ER}-IRES-GFP plasmid [9]. The cells were then FACS-sorted for GFP expression (FACSAria, Becton Dickinson). To generate murine MYC^{ER} cells, pBabepuro-MYC^{ER} plasmid (Addgene # 19128, provided by Dr. Wafik El-Deiry) [10] was used. The empty vector was used as control. pBabepuro-MYC^{ER} plasmid or empty vector was transfected into “Phoenix” retroviral packaging cells with TransIT®-LT1 Transfection Reagent (Mirus Bio, Madison, WI, USA). Primary murine PDAC target cells (PPT-5671, PPT-536361, PPT-8024, PPT-S559) all generated from murine *Ptf1a*$^{Cre/+}$*,LSL-Kras*^{G12D} PDACs, were transduced with retroviral particles with 8 µg/ml Polybrene (Merck Millipore, Darmstadt, Germany) and selected with 3 µg/mL Puromycin (Santa Cruz Biotechnology, Dallas, TX, USA).

Expression of MYC^{ER} was confirmed by immunoblotting. Cells stably expressing the MYC-ER fusion protein were treated with 500nM (human cells) or 600nM (murine cells) 4-OHT for time points indicated to activate MYC.

Murine PDAC cell lines ($Kras^{G12D}$-derived) PPT-5671 and PPT-53631 were genetically engineered to stably express MYC by retroviral transduction using the MSCV-MYC-IRES-GFP vector (Addgene # 18770, provided by Dr. Scott Lowe) [11]. Corresponding control cells were established using the MSCV-IRES-GFP empty vector (Addgene # 27490, provided by Dr. Warren Pear) [12]. The respective plasmids were transfected into “Phoenix Eco” retroviral packaging cells using Lipofectamine 2000 reagent (Thermo Fisher Scientific). The cells were then FACS-sorted for GFP expression (FACSAria, Becton Dickinson). Expression of MYC and GFP was confirmed by immunoblotting.

For lentiviral production of shRNAs, HEK 293T cells were transfected with lentiviral packaging plasmids (Addgene plasmid #12260 and #12259, both provided by Dr. Didier Trono) and plasmids containing murine *Ube2i* targeting shRNAs (#54: TRCN0000040839 and #56: TRCN0000040841)(Mission library, Sigma-Aldrich) or empty vector (Addgene plasmid #10878, provided by Dr. Bob Weinberg [13]). A knock-down was only detected with the shRNA #54: TRCN0000040839. The puromycin resistance has been subcloned to GFP, to allow FACS sorting. Lentivirus has been harvested in DMEM with 10% FCS and transductions were performed in the presence of 8µg/ml polybrene (Sigma-Aldrich).

Competitive repopulation assay

Murine PDAC cell lines PPT-5671 and PPT-53631 were retrovirally transduced to overexpress the MYC oncoprotein and the GFP reporter gene using the MSCV_MYC_IRES_GFP vector. Empty vector control lines, expressing GFP, were generated using the MSCV_IRES_GFP vector. For competitive repopulation experiments, PPT-5671 and PPT-53631 cells expressing the MYC oncogene together with GFP were mixed in a 20:80 ratio with parental cells (MYC+WT) and cultured for 5 days at 500nM ML-93 or a DMSO control in 6-well plates (total amount of cells: 5×10^5 cells per well). In analogy, GFP expressing control cells were mixed in a 20:80 ratio with wild type cells (control+WT) and cultured for 5 days and treated with

500nM ML-93 and DMSO accordingly. Cells were split 1:2 on d1 and d4. Medium, inhibitor and the DMSO control was replaced at each splitting. On day 5, FACS analysis (Beckman Coulter CyAn ADP LX) was performed to assess the fraction of GFP positive cells. The fold change in GFP positive cells was calculated as the ratio of GFP positive cells on d5 vs. d0 for both the MYC+WT and the control+WT setting. The fold change in GFP positive cells under SUMO inhibition with ML-93 for 5 days was normalized using the DMSO control for both MYC+WT and EV+WT and represented as normalized relative fold change in the manuscript.

Western blotting

Whole cell suspensions were lysed using specific lysis buffers with the final concentration: 50 mM Hepes, 150mM NaCl, 1 mM EDTA, 2.5 mM EGTA, 20 mM NEM, and 0.1 % Tween or RIPA buffer (150mM NaCl, NP-40 1% v/v, Sodium-deoxycholate 0.5%, SDS 0.1%, 25 mM Tris). For protein lysis, 900µl of the above described buffer were supplemented with 10µl PMSF (stock 100mM), 40µl suspension of 1:1ml diluted Roche Mini-Complete tablet, 2.5µl NaF (stock 0.4M) and 1µl of NaVO4 (stock 100mM) as protease inhibitors. Protein concentrations were assessed using Bradford reagent. Protein lysates were fractioned on SDS PAGE gels, transferred to Immobilon-P or Nitrocellulose (both from Millipore) membranes and incubated with specific primary antibodies. Primary and secondary antibodies and the thioester blots (Fig. S3B) are described below. Western blots were visualized by the Odyssey Infrared Imaging System (Licor, Bad Homburg, Germany) or the OPTIMAX X-Ray Film Processor (PROTEC, Oberstenfeld, Germany). For ECL measurement, western blots were incubated with HRP-linked secondary antibodies (GE Healthcare, USA) and SuperSignal™ West (ThermoFisher, USA) was used as HRP substrate. For ECL visualization CL-Xposure Film (ThermoFisher, USA) was used. Western blots were quantified using Odyssey software.

Immunoblotting antibodies

Protein	Company	Clone, Product #
SUMO1	Cell signaling, rabbit (1:1000)	21C7
SUMO2/3	Cell signaling, rabbit (1:1000)	8A2

c-MYC	Cell signaling	9402S
beta-Actin	SigmaAldrich	A5316, AC-15
RanGap1	Abcam	ab92360
alpha-tubulin	SigmaAldrich	T5168 B-5-1-2
beta-tubulin	Developmental Studies Hybridoma Bank	E7
GAPDH	Acris	ACR001PS
Secondary mouse IgG HRP Linked Whole Ab (1:10,000)	GE Healthcare	NA931V
Secondary rabbit IgG HRP Linked Whole Ab (1:10,000)	GE Healthcare	NA934V
Secondary Anti-rabbit IgG (H+L) (DyLight® 800 Conjugate)	Cell Signaling Technology	#5151
Secondary Anti-Mouse IgG (H+L) (DyLight® 700 Conjugate)	Cell Signaling Technology	#5470

Immunohistochemistry antibodies and conditions

<table>
<tr><td></td><td colspan="3">Immunohistochemistry protocols including machine; pretreatment condition; primary antibody; dilution; Detection Kit</td></tr>
<tr><td>Protein</td><td>MYC</td><td>Sumo1</td><td>Sumo2/3</td></tr>
<tr><td>Clinical PDAC cohort</td><td rowspan="2">BXT; CC1; abcam, ab32072; 1:50; Ultraview Detection Kit</td><td rowspan="3">Bond; ER2(40); DHSB Sumo1 76-86; 1:200; Polymer Refine Detection Kit</td><td rowspan="3">Bond; ER2(40); DHSB Sumo2 8A2; 1:200; Polymer Refine Detection Kit</td></tr>
<tr><td>Organoids</td></tr>
<tr><td>Xenograft tissues</td><td>Bond; ER1(30); abcam, ab32072; 1:50; Polymer Refine Detection Kit without post primary</td></tr>
</table>

For the IHC detection of Ki67 and cleaved Caspase3 of xenografted tissue the following antibodies were used:

Anti-Ki67 antibody [SP6] (ab16667), Abcam, Dilution 1:50

Cleaved Caspase-3 (Asp175) Antibody #9661, Cell Signaling, Dilution 1:150

RNA isolation and expression analysis

Expression levels were assessed with quantitative PCR as described [8]. In brief, RNA was isolated using the RNeasy kit (Qiagen, Hilden, Germany) or the Maxwell®16 Total RNA Purification Kit (Promega, Mannheim, Germany) and transcribed into cDNA with the Omniscript RT kit (Qiagen). qPCR was performed using a TaqMan cycler (Applied Biosystems, Applied Biosystems Inc., Carland, CA; USA) and the Platinum SYBR Green qPCR SuperMix-UDG kit (ThermoFisherScientific). Expression analysis was performed applying the ΔΔCt method.

qPCR Primers

Human: ODC1: Forward: 5`T C C T G G A G A G T T G C C T T T G T G A G A 3`; Reverse: 5`T C G A G G A A G T G G C A G T C A A A C T C T 3`; *CAD*: Forward: 5`T A G T C C T T G G C T C T G G C G T C T A 3`; Reverse: 5´T A G T C G G T G C T G A C T G T C T C T G 3`; *GAPDH*: Forward: 5`A A T C C C A T C A C C A T C T T C C A 3`; Reverse: 5`T G G A C T C C A C G A C G T A C T C A 3`; *SUMO1*: Forward: 5` T T C A A C T G A G G A C T T G G G G G 3` ; Reverse: 5´T G G A A C A C C C T G T C T T T G A C 3`; *SUMO2*: Forward: 5`G C C G A C G A A A A G C C C A A G G 3`; Reverse: 5` T G A C A A T C C C T G T C G T T C A C A A 3`; *MYC*: Forward: 5` T C A G A G T C T G G A T C A C C T T C T G C T 3`; Reverse: 5` TG C G T A G T T G T G C T G A T G T G T G G A 3`; *HSPE1*: Forward: 5` C A T C A T G T T G A T G C C A T T T C A 3`; Reverse: 5` T G G A G G C A C C A A A G T A G T T C T 3`; *SAE1*: Forward: 5`A C T G G A G C A G T G A G A A A G C A 3`; Reverse: 5` G C A G G T C A G G A C T A A T A C C C A 3`; *SAE2*: Forward: 5` A A C C T C C A G T T C C G T T G G A C 3`; Reverse: 5` T C C T G A G G T T T G C A G C A G A G 3`; *UBE2I*: Forward: 5` C C C A T T T G G T T T C G T G G C T G 3`, Reverse: 5` A C A T T T T G G T G G C G A A G A T G G 3`; *SUMO3*: Forward: 5` C C C A A G G A G G G T G T G A A G A C 3`; Reverse: 5` A T T G A C A A G C C C T G C C T C T C 3`.

Murine: *Myc*: Forward: 5` T T C C T T T G G G C G T T G G A A A C 3`; Reverse: 5`G C T G T A C G G A G T C G T A G T C G 3`; *Cad*: Forward: 5` C T G C C C G G A T T G A T T G A T G T C 3`; Reverse: 5` G G T A T T A G G C A T A G C A C A A A C C A 3`; *Odc1*: Forward: 5` A C A T C C A A A G G C A A A G T T G G 3`; Reverse: 5` A G C C T G C T G G T T T T G A G T G T 3`; *Gapdh*: Forward: 5` G G G T T C C T A T A A A T A C G G A C T G C 3`; Reverse: 5` T A C G G C C A A A T C C G T T C A C A 3'. *Ube2i:* Forward: 5` G G A A A G C C T G G A G G A A G G A C 3`; Reverse: 5` G A T G A A A C A G T G G G G G C T C A 3`;*Ubiquitin:* Forward: 5` G C A A G T G G C T A G A G T G C A G A G T A A 3`; Reverse: 5` T G G C T A T T A A T T A T T C G G T C T G C A T 3`; *Sae1*: Forward: 5` G C C C T G T A A A A G A G G C G C T A 3`; Reverse: 5` T G A T G C C C A G G G A G T C A A A C 3`; *Uba2/Sae2*: Forward: 5` C G C A A G A G G A A A C C T C C A G T 3`; Reverse: 5` T C T C C G C T A A A T G G A C T C G 3`.

UBE2I Thioester Western Blots

For thioester blots (SFig. 4), nonreducing SDS–PAGE was performed as recently described [14] and following antibodies were used: UBC9 (Epitomics, 2426-1), SUMO2/3 (monoclonal rabbit antibody generated by Takeda), UBCH10 (Boston Biochem, A650), and UBC12 (monoclonal mouse antibody generated by Takeda) used at a 1:1,000 dilution. The secondary Alexa 680–labeled antibody to rabbit/mouse IgG (1:5,000) were purchased from Invitrogen (A-21076, A-21058). Blots were imaged with a LI-COR Odyssey Infrared Imaging System. The ML93 concentration producing a half-maximal response (EC_{50}) were calculated using intensity values from LI-COR Immunoblot scans which were normalized to an α-tubulin loading control as described [14].

Biochemical and cellular assays of ML-93 activity

The ATP-inorganic pyrophosphate (PPi) exchange assay was carried out as described [14, 15]. Reactions were run using 2 nM SAE incubated with 1μM SUMO2 and 100 μM PPi

(containing 50 c.p.m./pmol [32P]PPi) in the presence of 1000 μM ATP. For assessment of cellular activity, HCT-116 cells were treated for 4h with increasing concentrations of ML-93, and 1 μM of ML-792 as a positive control, and assayed by Western blot hybridization for inhibition of formation of UBC9-SUMO thioester conjugates, UBC12-NEDD8 thioester conjugates, and UBC10-Ub thioester conjugates, as well as inhibition of global SUMOylation, as described [14].

Clinical PDAC patient cohort

Tissue microarrays of primary tumors in a primary resected human PDAC cohort were used to evaluate the protein expression in human tumor tissues. This cohort was investigated previously [16] and consists of 262 individuals that received partial pancreatoduodenectomy for PDAC between 1991 and 2006 at the Charité University Hospital, Berlin, Germany. Grading and staging followed the WHO recommendations at the time of cohort generation (TNM-classification of the 7thedition). The use of this tumor cohort for biomarker analysis has been approved by the Charité University ethics committee (EA1/06/2004). The tissue microarrays were generated as described [17, 18]. In short, three tumor cores (diameter 1.5 mm) of representative tumor areas selected by a board-certified pathologist on H&E stained slides were punched out of formalin-fixed paraffin embedded (FFPE) tissue blocks and arranged in a newly generated paraffin block.

Histological analysis and immunohistochemistry

Serial 2µm-thin sections prepared from paraffin blocks of embedded tissue and TMAs with a rotary microtome (HM355S, ThermoFisher Scientific, Waltham, USA) were collected and subjected to histological and immunohistochemical analysis. Hematoxylin-Eosin (H.-E.) staining was performed on deparaffinized sections with Eosin and Mayer's Haemalaun according to a standard protocol.

Immunohistochemistry was performed on automated staining systems (Ventana Benchmark XT (BXT), Ventana, Tucson, USA or Leica Bond Rxm (Bond), Leica, Wetzlar, Germany) with

different protocols (see Table in SM&M). Counterstaining was done with hematoxylin and a positive reaction, visible as a dark brown precipitate, was scored in a semiquantitative manner by two experienced comparative pathologists (AM and KS).

Clonogenic Assay

Human and murine PDAC cells were plated in medium containing ML-93 in 24-well plates for 5-7 days. Afterwards the medium was carefully removed from the wells and washed 3 times with PBS. The colonies were stained with 0.2% Crystal Violet solution (Sigma by Life Technologies TM, Darmstadt, Germany) for 20 minutes on a shaker at room temperature. To remove background staining, the wells were washed 3 times with tap water, dried and scanned. Afterwards Crystal Violet dye was solubilized in 1% SDS solution (Serva Electrophoresis GmbH, Heidelberg, Germany) and the absorbance at 570 nm was determined with a microplate reader (CLARIOstar, BMG Labtech, Ortenberg Germany). OD of vehicle treated controls was arbitrarily set to 1 and the therapeutic effect is depicted as relative colony formation.

Viability Assays and SUMO inhibitor treatment

PDAC cells were plated and after 24 hours treated with ML-93/ML-792. After 72 hours, viability of 2D culture cells was measured with an MTT assay in a 96-well format as described [6]. 3-(4,5-Dimethylthiazol-2-yl)-2,5-diphenyltetrazolium-bromid was purchased from Sigma (Munich, Germany) (10 mg/ml). In brief, 10 µL of the MTT dye was added per well followed by an incubation for 4 hours at 37°C. After media removal formazan crystals were dissolved in 200 µL DMSO:EtOH (v/v). Cell viability was determined by measuring the absorption at 595 nm in a Thermo/LabSystem Multiskan RC Microplate Reader (Artisan Technology Group, Champaign, IL, USA**).** In addition to MTT assay, cellular viability was measured by CellTiter-Glo ATP Viability Assay. In short, 25 µl CellTiter-Glo® Reagent (Promega) was added to each well of a 96-well plate after 72 hours of drug treatment. After 15 minutes of incubation on a shaker at room temperature, luminescence was measured on a FLUOstar OPTIMA microplate reader (BMG Labtech). Cellular viability of human PDAC organoids was determined using the

CellTiter-Glo® 3D ATP Viability Assay according to the protocol of the manufacturer (Promega). Viability was determined by measuring luminescence on a FLUOstar OPTIMA microplate reader (BMG Labtech, Ortenberg, Germany). Viability was measured 3 days (2D culture) or 5 days (organoid culture) after the addition of the drug. The OD or luminescence of vehicle-treated controls was arbitrary set to 1 and the dose-response is depicted as relative viability. To determine the ML-792 and ML-93 dose response curves a seven-point drug dilution was used.

Annexin V-, Cell Cycle-FACS, Viability analysis by FACS

Induction of apoptosis via SUMO inhibition was assessed by either Annexin V/propidium iodide (PI) or Annexin V/4′,6-Diamidino-2-phenylindole dihydrochloride (DAPI) flow cytometric analysis depending on the cell lines investigated. Briefly, ML-93 and DMSO treated cells were stained with APC Annexin-V (Biolegend®, Cat: 640941) or PI (Sigma-Aldrich). Transgenic cell lines expressing the GFP reporter gene were stained with APC Annexin-V (Biolegend®, Cat: 640941) and DAPI (Thermo Fisher Scientific) to minimize spectral overlap. The apoptotic fraction was defined as Annexin V-positive/propidium iodide-negative cells. For cell lines expressing the GFP reporter gene, the apoptotic fraction was defined as the Annexin V-positive/DAPI-negative cells, respectively. Propidium iodide-positive and DAPI-positive cells were deemed to be necrotic cells regardless of their Annexin V staining properties. Annexin-V-negative/propidium iodide-negative as well as annexin-V-negative/DAPI-negative cells were classified as viable cells. PDAC cells were treated with ML-93 or DMSO control for the indicated time point, fixed in ice-cold ethanol (70%) and resuspended in propidium iodide and RNase A (Qiagen, Hilden, Germany) in phosphate-buffered saline. The proportion of cells in each cell cycle phase was determined using flow cytometric assessment of DNA content (*CyAn* ADP *Lx,* Becton Dickinson, San Jose, CA, USA). Analysis of data were performed using FlowJo™ (FlowJo, LLC Ashland, OR, USA) software.

Generation of in vivo xenografts and SUMO inhibitor toxicity

All animal experiments were performed in accordance with regional Gothenburg University animal ethics committee approval 100/16 and 5.8.18-01949/2018 and approval of Regierung von Oberbayern ROB-55.2-2532.Vet_02-17-230. The tumor cells were suspended in RPMI, mixed 1:1 with Matrigel (BD Biosciences) and transplanted subcutaneously onto the flanks of immunocompromised, non-obese severe combined immune deficient interleukin-2 chain receptor γ knockout mice (NOG mice; Taconic, Denmark) (PaTu-8988T, PSN1, BxPc3, and IMIM-PC1 lines) or NOD.CB17-Prkdcscid/NCrCrl mice (NOD SCID mice; Charles river, Italy) (HuPDAC7 cell line). $1x10^6$ cells were used for PaTu-8988T, PSN1, BxPc3, and IMIM-PC1 lines, $2x10^6$ cells were used for the HuPDAC7 line. Mice were weighted and tumors measured using calipers twice a week. The metric tumor volume (V) was calculated by measurements of length (L) and width (W) by applying the following equation: $V = 0.5 \times (L \times W^2)$. Treatments were started when the tumors were actively growing, judged by increasing volumes on repeated caliper measurements. ML-93 was dissolved in beta hydroxypropyl cyclodextrin and mice were dosed intravenously with 50mg/kg body weight per dose. Dosing regimen for intravenous delivery were two consecutive days per week. Tumor size was measured until best response, or until no further effects could be expected. Mice were sacrificed before or when tumors reached ethical size limit. For *in vivo* testing of ML-93 toxicity, female C57Bl6/J mice were treated with 50 mg/kg ML-93 or vehicle control on day 1 and 2. On day 8 blood samples were analysed on a blood counter (scil Animal Blood Counter, USA) and single cell suspensions from spleens were generated (100µM cell strainer). Following red blood cell lysis (ACK Lysing Buffer, GIBCO, Thermo Fisher Scientific), splenocytes were snap frozen for consecutive western blot analysis and processed following the described protein lysis protocol.

Proteome analysis by mass spectrometry

Sample preparation

Human PDAC cell lines PATU-8988T and PSN1 were treated with 500nM of SUMOi for 48h in triplicates. Cells were lysed in 2% SDS lysis buffer, shortly heated to 95 °C, then sonicated and centrifuged at 16000 g for 5 minutes. In the following, protein content was determined

using the DC Protein Assay Kit from BioRad. For in-solution digest, 20 µg of each sample was precipitated using 4 volumes of acetone for 1 hour at -20 °C. After centrifugation a wash step with 90% acetone was included. The precipitated pellet was shortly dried at room temperature and then resuspended in 6M urea/2M thiourea. Proteins were reduced with DTT, following an alkylation step using chloroacetamide. Digestion was performed in only 2M urea with the endopeptidase Lys-C (Wako) in combination with trypsin (sequence grade, Promega) overnight at 37 °C. Digestion was stopped by acidifying. Finally, peptides were desalted and concentrated by the STAGE tipping technique (Stop and Go Extraction) described by Rappsilber et al. [19].

Liquid chromatography and mass spectrometry

LC-MS/MS analysis was performed utilizing an Easy-nLC II via a nano-electrospray ionization source to the Orbitrap Elite mass spectrometer. Peptides were separated according to their hydrophobicity on an in-house packed 17 cm long 75µm ID column with 3 µm C18 beads (Dr Maisch GmbH). The binary buffer system used consisted of solution A: 0.1% formic acid and solution B: 80% acetonitrile, 0.1% formic acid. For proteome analysis, a linear gradient of 120 minutes was used (0-120 min, 33% B). Then the concentration of solution B was increased to 50% in 5 minutes and finally increased to 95% in 5 minutes.

Orbitrap Elite settings: MS spectra were acquired with a maximal injection time of 100 ms, a resolution of 120000 at 200 m/z and $1x10^6$ as an AGC target. MS/MS spectra of the top 20 most intense peaks were obtained by collision-induced dissociation (CID) in the ion trap. The maximal injection time was set to 25 ms, with an AGC target of $5x10^3$ and a rapid scan mode.

Data Analysis

The acquired raw files were processed in one single run using the MaxQuant software (version 1.5.8.0) and its implemented Andromeda search engine [20, 21]. Assignment of proteins was achieved by correlation of electrospray ionization-tandem mass spectrometry (ESI-MS/MS) fragmentation spectra with the Uniprot human database (version 2017), additionally including

a list of common contaminants. All searches were performed using default settings for mass tolerances for MS and MS/MS spectra. Tryptic specifications were chosen. Carbamidomethyl at cysteine residues was set as fixed modification whereas oxidation at methionine and acetylation at the N-terminus were chosen as variable modifications. Further, the false discovery rate for proteins and peptide-spectrum matches was set to 1% as default and the minimal peptide length was defined to be seven amino acids. Proteins were quantified using the integrated MaxLFQ algorithm [22], allowing only unique peptides for quantification and retaining unmodified counterpart peptides. The minimum LFQ ratio count was set to 2, FastLFQ was enabled and the number of minimal unique peptides was set to 1 for identification. Furthermore, the match-between-run feature was used with a time window set to 0.7 minutes.

The Perseus software (version 1.5.8.5) was used for downstream analysis of the data. Using the filter option, contaminants, reverse entries and proteins only identified by a modified peptide were removed. In the following, LFQ intensities were logarithmized and normal distribution of the LFQ values was ensured by visual histogram analysis. Correlation of triplicates was checked by multiscatter plot analysis. For statistical analysis, triplicates were grouped into one group and the significant difference of two sample groups was tested using the Student's t-test as a two-sample test.

RNAseq analysis

For RNA-seq of 4-OHT treated IMIM-PC1 cells, an Illumina TruSeq Stranded RNA Library Prep Kit was used and further analyzed on an Illumina HiSeq2000 system (DKFZ Heidelberg NGS core facility). Resulting Fastq files were obtained from DKFZ Heidelberg NGS core facility (approximately 25M reads/sample (single-end reads)) and further processed and analyzed using the Galaxy Project platform [23]. First, adapters were removed from Fastq files using TrimGalore! (Galaxy version 0.4.3.1), afterwards sequencing-reads were mapped to the human reference genome hg19 (GRCh37) using Bowtie2 (Galaxy version 2.3.2.2) [24] and annotated with the hg19 GTF annotation file, obtained from the UCSC genome browser

database [25]. Differential expression of count data (htseq-count 0.6.1galaxy3) was determined by DESeq2 (Galaxy version 2.11.39) [26, 27].

Human BxPC3, Pa-Tu-8988T, PSN1 with and without ML-93 treatment were analyzed in triplicates. Murine 53631PPT cells retroviral tranduced with a hMYC-cDNA expression vector and the respective control with and without ML-93 treatment were analzed in quintuplicates. To verify positive integration of pDNA hMYC-cDNA, IRES and GFP a respective fasta file has been generated and been mapped to all murine samples using bowtie2 [17] and visualized by IGV [28]. Library preparation for bulk 3'-sequencing of poly(A)-RNA was done as described previously [29]. Briefly, barcoded cDNA of each sample was generated with a Maxima RT polymerase (Thermo Fisher) using oligo-dT primer containing barcodes, unique molecular identifiers (UMIs) and an adapter. 5' ends of the cDNAs were extended by a template switch oligo (TSO) and full-length cDNA was amplified with primers binding to the TSO-site and the adapter. cDNA was tagmented with the Nextera XT kit (Illumina) and 3'-end-fragments finally amplified using primers with Illumina P5 and P7 overhangs. In comparison to Parekh et al. the P5 and P7 sites were exchanged to allow sequencing of the cDNA in read1 and barcodes and UMIs in read2 to achieve a better cluster recognition. The library was sequenced on a NextSeq 500 (Illumina) with 75 cycles for the cDNA in read1 and 16 cycles for the barcodes and UMIs in read2. Data was processed using the published Drop-seq pipeline (v1.0) to generate sample- and gene-wise UMI tables [30]. Reference genomes (GRCm38, murine; GRCh37, human) were used for alignment. Transcript and gene definitions were used according to the ENSEMBL annotation release 75. Accession numbers: GSE119423, PRJNA489233 and PRJEB34637. In addition, we used a RNA-seq dataset of 38 murine PDAC cancer cell lines that was recently described [3] and can be accessed via ENA: PRJEB23787. mRNA expression profiles of conventional human PDAC cell lines were from the Cancer Cell Line Encyclopedia [31] and downloaded via the cBioPortal platform (http://www.cbioportal.org) [32].

Gene expression profiling, gene set enrichment analysis, transcriptomics and genomics data analysis

Normalized gene expression and clinical data, corresponding to Fig. 2F, were obtained from Bailey et al. (nature16965-s2) [33]. Gene expression values were transformed into z-scores (indicating the deviation from the population mean in units of standard deviation) for each gene and sample in comparison to all the other samples. For a clearer representation in the heat map, the range of z-scores is split into six intervals, each corresponding to a distinct color. For different classes of tumor subtypes and degrees of differentiation, we used Fisher's Exact Test to test for their respective enrichment. For gene set enrichment analysis (GSEA), we used GeneTrail2 1.6 [34]. A detailed description of the unweighted GSEA performed by GeneTrail2 1.6 can be found below. In addition to GeneTrail2, we accessed the GSEAsoftware v.3.0 via the Broad Institute (www.broadinstitute.org) to perform gene set enrichment analysis [35]. Statistical values (nominal p-value, FDR q-value) are indicated. TCGA PAAD mRNA expression data and clinical data sets were accessed via UCSC cancer genomics browser [36]. The 75^{th} and 25^{th} percentile, were defined as thresholds for "high" and "low" expression. TCGA PDAC survival data for UBE2I, SUMO1, SUMO2, and SUMO3 were accessed and plotted via the OncoLnc webpage (http://www.oncolnc.org/) [37]. Genomics data for CNA analysis was assessed using the cBioPortal online platform [32, 38]. Genes regulated by ML-93 in human PDAC lines (log FC +/- 0.58, FDR<0.05) were analyzed using the Hallmark gene sets of the MSigDB. Pearson correlation of ML-792 and ML-93 GI_{50} to mRNA expression is described in SM&M. The Pearson correlation coefficient was used as a rank to run a pre-ranked GSEA with the GSEA 4.0.1 software.

Unweighted GSEA by GeneTrail2

To assess altered biological pathways and processes in the $SUMO^{high}$ group in comparison to the $SUMO^{low}$ group, scores of differential expression were computed using Independent Shrinkage t-Test [39] and an unweighted Gene Set Enrichment Analysis was performed on a variety of functional categories using the GeneTrail2 web service [34].

GeneTrail2 is a comprehensive web service providing access to different tools for the statistical analysis of molecular signatures with a focus on enrichment analyses. These include the well-known weighted gene set enrichment analysis (GSEA), which has been developed by Subramanian et al. [35] (Broad Institute, www.broadinstitute.org), as well as an unweighted version of GSEA. In the classical (weighted) GSEA, p-values are typically computed using permutation-based approaches, which are limited to p-values as small as 1/(number of permutations). In contrast to this, the unweighted GSEA allows for exact p-value computation based on a dynamic programming algorithm [40]. Besides lower runtimes, the exact p-value assessment has the major advantage that extremely significant results can be better distinguished from marginally significant ones.

The main difference between the weighted and the unweighted GSEA lies in the computation of the running sum statistic, which in the former case additionally assigns a weight to each gene, mirroring its correlation with the phenotype. This distinction is also reflected in the corresponding running sum plots.

As a multitude of gene sets are tested simultaneously in exploratory enrichment analyses, the obtained p-values need to be corrected for multiple-hypothesis testing to prevent the accumulation of type-1 error. As correction for multiple hypothesis testing, we used the method by Benjamini and Yekutieli [41] as provided by GeneTrail2, resulting in the indicated q-values.

Correlation of GI_{50} values with mRNA expression

The sensitivity to SUMO inhibitors ML792 and ML793 across murine pancreatic cancer cell lines (n=38, only $Kras^{G12D}$-driven lines) was correlated with gene expression obtained by RNA-seq [3]. GI_{50} values were used as a measure of drug sensitivity and log2-counts per million computed using the edgeR-limma pipeline from the Bioconductor Project [42, 43, 44] served as a measure of gene expression. Correlation coefficients were calculated using the Pearson method.

References Supplemental Methods

1 von Burstin J, Eser S, Paul MC, Seidler B, Brandl M, Messer M*, et al.* E-cadherin regulates metastasis of pancreatic cancer in vivo and is suppressed by a SNAIL/HDAC1/HDAC2 repressor complex. Gastroenterology 2009;**137**:361-71, 71 e1-5.

2 Eser S, Reiff N, Messer M, Seidler B, Gottschalk K, Dobler M*, et al.* Selective requirement of PI3K/PDK1 signaling for Kras oncogene-driven pancreatic cell plasticity and cancer. Cancer Cell 2013;**23**:406-20.

3 Mueller S, Engleitner T, Maresch R, Zukowska M, Lange S, Kaltenbacher T*, et al.* Evolutionary routes and KRAS dosage define pancreatic cancer phenotypes. Nature 2018;**554**:62-8.

4 Ossewaarde JM, de Vries A, Bestebroer T, Angulo AF. Application of a Mycoplasma group-specific PCR for monitoring decontamination of Mycoplasma-infected Chlamydia sp. strains. Appl Environ Microbiol 1996;**62**:328-31.

5 Boj SF, Hwang CI, Baker LA, Chio, II, Engle DD, Corbo V*, et al.* Organoid models of human and mouse ductal pancreatic cancer. Cell 2015;**160**:324-38.

6 Hassan Z, Schneeweis C, Wirth M, Veltkamp C, Dantes Z, Feuerecker B*, et al.* MTOR inhibitor-based combination therapies for pancreatic cancer. Br J Cancer 2018;**118**:366-77.

7 Conradt L, Godl K, Schaab C, Tebbe A, Eser S, Diersch S*, et al.* Disclosure of erlotinib as a multikinase inhibitor in pancreatic ductal adenocarcinoma. Neoplasia 2011;**13**:1026-34.

8 Hoellein A, Fallahi M, Schoeffmann S, Steidle S, Schaub FX, Rudelius M*, et al.* Myc-induced SUMOylation is a therapeutic vulnerability for B-cell lymphoma. Blood 2014;**124**:2081-90.

9 Franke K, Vilne B, Prazeres da Costa O, Rudelius M, Peschel C, Oostendorp RA*, et al.* In vivo hematopoietic Myc activation directs a transcriptional signature in endothelial cells within the bone marrow microenvironment. Oncotarget 2015;**6**:21827-39.

10 Ricci MS, Jin Z, Dews M, Yu D, Thomas-Tikhonenko A, Dicker DT*, et al.* Direct repression of FLIP expression by c-myc is a major determinant of TRAIL sensitivity. Mol Cell Biol 2004;**24**:8541-55.

11 Hemann MT, Bric A, Teruya-Feldstein J, Herbst A, Nilsson JA, Cordon-Cardo C*, et al.* Evasion of the p53 tumour surveillance network by tumour-derived MYC mutants. Nature 2005;**436**:807-11.

12 Pear WS, Miller JP, Xu L, Pui JC, Soffer B, Quackenbush RC*, et al.* Efficient and rapid induction of a chronic myelogenous leukemia-like myeloproliferative disease in mice receiving P210 bcr/abl-transduced bone marrow. Blood 1998;**92**:3780-92.

13 Stewart SA, Dykxhoorn DM, Palliser D, Mizuno H, Yu EY, An DS*, et al.* Lentivirus-delivered stable gene silencing by RNAi in primary cells. RNA 2003;**9**:493-501.

14 He X, Riceberg J, Soucy T, Koenig E, Minissale J, Gallery M*, et al.* Probing the roles of SUMOylation in cancer cell biology by using a selective SAE inhibitor. Nat Chem Biol 2017;**13**:1164-71.

15 Bruzzese FJ, Milhollen MA, Gavin JM, Josephine HR, Brownell JE. Identification and application of NEDD8 E1 inhibitors. Methods Mol Biol 2012;**832**:577-88.

16 Muckenhuber A, Berger AK, Schlitter AM, Steiger K, Konukiewitz B, Trumpp A*, et al.* Pancreatic Ductal Adenocarcinoma Subtyping Using the Biomarkers Hepatocyte Nuclear Factor-1A and Cytokeratin-81 Correlates with Outcome and Treatment Response. Clin Cancer Res 2018;**24**:351-9.

17 Noll EM, Eisen C, Stenzinger A, Espinet E, Muckenhuber A, Klein C*, et al.* CYP3A5 mediates basal and acquired therapy resistance in different subtypes of pancreatic ductal adenocarcinoma. Nat Med 2016;**22**:278-87.

18 Stenzinger A, Endris V, Klauschen F, Sinn B, Lorenz K, Warth A*, et al.* High SIRT1 expression is a negative prognosticator in pancreatic ductal adenocarcinoma. BMC Cancer 2013;**13**:450.

19 Rappsilber J, Ishihama Y, Mann M. Stop and go extraction tips for matrix-assisted laser desorption/ionization, nanoelectrospray, and LC/MS sample pretreatment in proteomics. Anal Chem 2003;**75**:663-70.

20 Cox J, Mann M. MaxQuant enables high peptide identification rates, individualized p.p.b.-range mass accuracies and proteome-wide protein quantification. Nat Biotechnol 2008;**26**:1367-72.

21 Cox J, Michalski A, Mann M. Software lock mass by two-dimensional minimization of peptide mass errors. J Am Soc Mass Spectrom 2011;**22**:1373-80.

22 Cox J, Hein MY, Luber CA, Paron I, Nagaraj N, Mann M. Accurate proteome-wide label-free quantification by delayed normalization and maximal peptide ratio extraction, termed MaxLFQ. Mol Cell Proteomics 2014;**13**:2513-26.

23 Afgan E, Baker D, van den Beek M, Blankenberg D, Bouvier D, Cech M*, et al.* The Galaxy platform for accessible, reproducible and collaborative biomedical analyses: 2016 update. Nucleic Acids Res 2016;**44**:W3-W10.

24 Langmead B, Salzberg SL. Fast gapped-read alignment with Bowtie 2. Nat Methods 2012;**9**:357-9.

25 Casper J, Zweig AS, Villarreal C, Tyner C, Speir ML, Rosenbloom KR*, et al.* The UCSC Genome Browser database: 2018 update. Nucleic Acids Res 2018;**46**:D762-D9.

26 Anders S, Pyl PT, Huber W. HTSeq--a Python framework to work with high-throughput sequencing data. Bioinformatics 2015;**31**:166-9.

27 Love MI, Huber W, Anders S. Moderated estimation of fold change and dispersion for RNA-seq data with DESeq2. Genome Biol 2014;**15**:550.

28 Robinson JT, Thorvaldsdottir H, Winckler W, Guttman M, Lander ES, Getz G*, et al.* Integrative genomics viewer. Nat Biotechnol 2011;**29**:24-6.

29 Parekh S, Ziegenhain C, Vieth B, Enard W, Hellmann I. The impact of amplification on differential expression analyses by RNA-seq. Sci Rep 2016;**6**:25533.

30 Macosko EZ, Basu A, Satija R, Nemesh J, Shekhar K, Goldman M*, et al.* Highly Parallel Genome-wide Expression Profiling of Individual Cells Using Nanoliter Droplets. Cell 2015;**161**:1202-14.

31 Barretina J, Caponigro G, Stransky N, Venkatesan K, Margolin AA, Kim S*, et al.* The Cancer Cell Line Encyclopedia enables predictive modelling of anticancer drug sensitivity. Nature 2012;**483**:603-7.

32 Cerami E, Gao J, Dogrusoz U, Gross BE, Sumer SO, Aksoy BA*, et al.* The cBio cancer genomics portal: an open platform for exploring multidimensional cancer genomics data. Cancer Discov 2012;**2**:401-4.

33 Bailey P, Chang DK, Nones K, Johns AL, Patch AM, Gingras MC*, et al.* Genomic analyses identify molecular subtypes of pancreatic cancer. Nature 2016;**531**:47-52.

34 Stockel D, Kehl T, Trampert P, Schneider L, Backes C, Ludwig N*, et al.* Multi-omics enrichment analysis using the GeneTrail2 web service. Bioinformatics 2016;**32**:1502-8.

35 Subramanian A, Tamayo P, Mootha VK, Mukherjee S, Ebert BL, Gillette MA*, et al.* Gene set enrichment analysis: a knowledge-based approach for interpreting genome-wide expression profiles. Proc Natl Acad Sci U S A 2005;**102**:15545-50.

36 Cline MS, Craft B, Swatloski T, Goldman M, Ma S, Haussler D*, et al.* Exploring TCGA Pan-Cancer data at the UCSC Cancer Genomics Browser. Sci Rep 2013;**3**:2652.

37 Anaya J. OncoLnc: linking TCGA survival data to mRNAs, miRNAs, and lncRNAs. PeerJ Comput Sci 2016;**2**:e67.

38 Gao J, Aksoy BA, Dogrusoz U, Dresdner G, Gross B, Sumer SO*, et al.* Integrative analysis of complex cancer genomics and clinical profiles using the cBioPortal. Sci Signal 2013;**6**:pl1.

39 Opgen-Rhein R, Strimmer K. Accurate ranking of differentially expressed genes by a distribution-free shrinkage approach. Stat Appl Genet Mol Biol 2007;**6**:Article9.

40 Keller A, Backes C, Lenhof HP. Computation of significance scores of unweighted Gene Set Enrichment Analyses. BMC Bioinformatics 2007;**8**:290.

41 Benjamini Y, Drai D, Elmer G, Kafkafi N, Golani I. Controlling the false discovery rate in behavior genetics research. Behav Brain Res 2001;**125**:279-84.

42 Robinson MD, McCarthy DJ, Smyth GK. edgeR: a Bioconductor package for differential expression analysis of digital gene expression data. Bioinformatics 2010;**26**:139-40.

43 Ritchie ME, Phipson B, Wu D, Hu Y, Law CW, Shi W*, et al.* limma powers differential expression analyses for RNA-sequencing and microarray studies. Nucleic Acids Res 2015;**43**:e47.

44 Huber W, Carey VJ, Gentleman R, Anders S, Carlson M, Carvalho BS*, et al.* Orchestrating high-throughput genomic analysis with Bioconductor. Nat Methods 2015;**12**:115-21.

Supplemental Figure Legends

Supplemental Figure 1. The SUMOylation pathway is deregulated in PDAC.

A Gene expression analysis (z-transformed; GSE 62452) reveals a significant enrichment of core SUMO pathway components within PDAC patients vs. healthy control tissue.

B Unweighted GSEA demonstrates significant enrichment of established SUMOylation-associated gene sets in PDAC patients vs. healthy controls (GO PROTEIN SUMOYLATION; GO SUMO TRANSFERASE ACTIVITY).

C Unweighted GSEA of *SUMO1, SUMO2,* or *SUMO3* mRNA high (>75th percentile) and low (<25th percentile) expressing PDACs (TCGA-PAAD dataset). q-value is depicted.

D Unweighted GSEA of a publicly available dataset (GSE36924) indicates significant enrichment of MYC hallmark target genes within the SUMO^{high} group vs. SUMO^{low} group.

E SUMO-high group, depicted in blue, reveals a worse overall survival (p=0.011) and progression-free-survival (p=0.005).

Supplemental Figure 2. MYC is connected to the core Sumo pathway in murine PDAC.

A *Myc* mRNA expression of murine PDAC cell lines (PRJEB23787 dataset) (n=38) were correlated with the mRNA expression of the core Sumo pathway genes *Sumo1*, *Sumo2*, *Sumo3*, *Ube2i*, *Sae1*, and *Uba2/Sae2*. The color-coded Pearson correlation coefficient r is provided. *** p<0.001, ** p<0.01

B GSEA of a publicly available data set (GSE77328) reveals loss of SUMO transcriptional signature in KRAS/p53mut-driven PDAC under OmoMYC-mediated suppression of MYC compared to MYC active controls.

Supplemental Figure 3. Specificity and potency of SUMOi

A Six human PDAC cells were treated for 72 hours with the indicated concentrations of ML-792. Viability was measured with MTT assays. Vehicle treated controls were arbitrarily set to 1.

Biederstädt A, *et al. Gut* 2020;0:1–11. doi: 10.1136/gutjnl-2018-317856

B To test the potency and selectivity of ML-93 in cells, HCT-116 cells were treated for 4h with increasing concentrations of ML-93, and 1 μM of ML-792 as a positive control, and assayed by Western blot hybridization for inhibition of formation of UBC9-SUMO thioester conjugates (UBC9 is the E2 enzyme in the SUMO pathway), UBC12-NEDD8 thioester conjugates (UBC12 is the E2 enzyme in the NAE pathway), and UBC10-Ub thioester conjugates (UBC10 is an E2 enzyme in the UAE pathway), as well as inhibition of global SUMOylation.

Supplemental Figure 4. Characterization of the SUMOi.

A, B Clonogenic growth of the depicted six human PDAC cell lines treated with increasing ML-93 doses. **A** representative experiment. **B** quantification of clonogenic growth of at least three independent experiment. ANOVA *p<0.05, **p<0.01, ***p<0.001, ****p<0.0001

C, D ML-93 induces cell cycle alteration, polyploidization, and apoptosis in **C**: PSN1 and **D**: PaTu-8988T cells as demonstrated by PI cell cycle flow cytometry analyses. Shown are the proportions of cells in the sub G1-, G1-, and G2/M- phase 48 hours after ML-93 treatment (50 nM). All biological replicates (PSN1: n=3; PaTu-8988T: n=5) were performed as technical triplicates. Shown is the mean +/- SD and statistical significance was assessed using Student's t-test.

Supplemental Figure 5. On target activity and pathways regulated by ML-93

A ML-93 long-term effects on specific target SUMOylation (144 hours). ML-93 treatment with the indicated doses stabilizes the endogenous non-SUMOylated form of RanGap1 in PaTu-8988T cells.

B RNA-seq expression profiles of PaTu-8988T cells treated with 500nM ML-93 for 24h or left as vehicle treated controls were analyzed by GSEA. NES: normalized enrichment score, p: nominal p-value, FDR: false discovery rate q-value.

Biederstädt A, *et al. Gut* 2020;0:1–11. doi: 10.1136/gutjnl-2018-317856

C Venn diagrams depict the overlap in both downregulated as well as upregulated genes under SUMOylation inhibition with ML-93. RNA-seq in BxPc3, PaTU-8988T, and PSN1 was performed 24h after the ML-93 treatment.

D Genes significantly regulated upon ML-93 treatment (log FC +/- 0.58, FDR<0.05) were analyzed with the Molecular Signature Database. Venn diagrams of pathways associated with up and downregulated genes.

E Common HALLMARK signature associated with ML-93 up- or down-regulated genes (corresponding to D). The color-coded FDR q-value is shown for each line and signature.

F Global proteomic analysis of human PDAC cell lines PaTu-8988T and PSN1 was performed after treatment with 500 nM ML-93 for 48h. Depicted are proteins, which are exclusively expressed in control or ML-93 treated cells as well as an overlap of both cell lines. Changes in the proteome were visualized by plotting the difference of the log2 mean protein intensities between the ML-93 treatment and DMSO control against the negative logarithmized p-values. Proteins with 2-fold change and a p-value < 0.05 are considered high-confidence hits (designated in red as significantly regulated). Measurements were made each in triplicates.

Supplemental Figure 6. SUMO inhibitor activity in PDAC cells and association to MYC

A Human conventional PDAC cell lines with quantified MYC protein expression were analyzed by GSEA. High expression: MYC protein expression >66th percentile; Low expression: MYC protein expression <66th percentile (according to Fig. 3C). NES: normalized enrichment score, p: nominal p-value, FDR: false discovery rate q-value.

B, C mRNAs from a RNA-seq expression dataset of 38 murine PDAC cell lines were correlated with the GI_{50} values for ML-93 and ML-792. The Pearson correlation coefficient was used as a rank to run a pre-ranked GSEA. B, Venn diagram of HALLMARK signatures associated with GI_{50} negative correlated genes. The common signatures for ML-93 and ML-792 are depicted. C, Enrichment blots for both HALLMARK

Biederstädt A, *et al. Gut* 2020;0:1–11. doi: 10.1136/gutjnl-2018-317856

MYC signatures for both SUMO inhibitors. NES: normalized enrichment score, p: nominal p-value, FDR: false discovery rate q-value.

Supplemental Figure 7. SUMO inhibitor activity in PDAC cells and association to MYC

A Murine PPT-8024, PPT-5671, PPT-53631, and PPT-S559 PDAC cell lines were transduced with an MYC^{ER} vector or an empty control vector (PPT-53631). MYC western blot to demonstrate expression of MYC^{ER}. actin: loading control.

B The indicated murine cell lines were treated with 4-OHT (600 nM) for 8 hours or were left as vehicle treated control. qPCR analysis for *Myc*, *Odc1*, *Cad, Sae1,* and *Uba2/Sae2* mRNA expression. *Gapdh* mRNA was used for normalization. Shown is the mean +/- SD of three independent experiments performed as technical triplicates.

C, D Murine PPT-8024, PPT-5671, PPT-53631 PDAC cell lines were transduced with an MYC^{ER} vector or an empty control vector (PPT-53631). **C**, Cell were treated with 4-Hydroxytamoxifen (4-OHT) (600 nM) or vehicle control and increasing doses of ML-93 as indicated. **C**, Viability was measured after 72 hours with MTT assays and dose-response curves are depicted. Each experiment represents at least three biological replicates performed as triplicates. Shown is the mean +/- SD. * t-test $p<0.05$. **D**, Shows representative experiments of clonogenic assays (upper panel) and the corresponding quantification (lower panel). Each experiment represents at least three biological replicates performed as duplicates. Shown is the mean +/- SD. t-test *$p<0.05$, **$p<0.01$, ***$p<0.001$, ****$p<0.0001$.

E Cells described in A-D were treated with 4-Hydroxytamoxifen (600 nM) or vehicle control and increasing doses of ML-792 as indicated. Shown are representative experiments of clonogenic assays.

F Human IMIM-PC1^{MYCER} cells were treated with 4-Hydroxytamoxifen (500 nM) or vehicle control and increasing doses of ML-93 or ML-792 as indicated. Viability was measured after 72 hours with MTT assays and dose-response curves are depicted. Each

Biederstädt A, *et al. Gut* 2020;0:1–11. doi: 10.1136/gutjnl-2018-317856

experiment was performed: ML-93 n=4, ML-792 n=2; experiments were done as triplicates. Shown is the mean +/- SD. * t-test p<0.05.

G PPT-S559^{MYCER} cells were treated with 4-OHT (600 nM) for 8 hours or were left as vehicle treated control. qPCR analysis for *Myc*, *Odc1*, *Cad, Sae1, and Sae2* mRNA expression. *Gapdh* mRNA was used for normalization. Shown is the mean +/- SD of three independent experiments performed as technical triplicates.

H,I Murine PPT-S559^{MYCER} cells were transduced with either *Ube2i* shRNA or an empty vector control, both co-expressing GFP. **H**, to assess *Ube2i* knockdown efficacy, viable GFP+ cells were FACS-sorted and *Ube2i* mRNA expression was quantified and normalized to *Ubiquitin*. Two independent experiments were analyzed. **I**, Cells were treated with 4-Hydroxytamoxifen (4-OHT) (600 nM) or vehicle control and viability of GFP-positive cells was measured after 72 hours with DAPI staining. GFP/DAPI double positive cells were assessed by flow cytometry. The relative fold change was measured as the relative difference in the fraction of GFP/DAPI double positive cells in vehicle control versus 4-OHT treated cells. The experiment represents three biological replicates. Shown is the mean +/- SD. Unpaired t-test *p<0.05.

Supplemental Figure 8. *In vivo* testing of ML-93

A ML-93 treatment schedule used for the *in vivo* toxicity analysis in C57BL/6 mice.

B Body weight of control (n=6) and ML-93 (n=6) treated mice at day 1 and day 8.

C Blood cell parameters, hemoglobin, white blood cells, and thrombocytes of control and ML-93 treated mice at day 8.

D ML-93 treatment schedule to determine on-target efficacy of ML-93 in protein lysates of splenocytes.

E SUMO2/3 western blot in splenocyte lysates of four control and four ML-93 treated mice. actin: loading control.

F, G Immunodeficient mice were treated with 50mg/kg ML-93 intravenously on d1,2 and d8,9 (**F**) and tumor size of PSN1 (control n=3 mice; ML-93 n=5 mice), HuPDAC7

(control n=5 mice; ML-93 n=5 mice), BxPc3 (control n=3 mice; ML-93 n=3 mice), and IMIM-PC1 (control n=3 mice; ML-93 n=3 mice)-derived tumors was measured over time (**G**).

H-J Immunodeficient mice were treated with 50mg/kg ML-93 intravenously on d1,2 and tumor tissue for IHC was prepared at d3 (**H**). Percent Ki67 (**I**) and cleaved caspase3 (**J**) of two control mice and two ML-93 treated mice were compared. * p value of an unpaired t-test <0.05.

Supplemental Figure 9. SUMOi activity in primary human PDAC models.

A Patient-derived organoids were treated with increasing doses of ML-93 for five days and cellular viability was assessed using ATP levels as a readout for viability. All replicates were performed as technical triplicates.

B mRNA expression based on RNA-seq of the four analyzed human PDAC organoid lines for the indicated transcripts. mRNA expression Z-score is color coded.

C Quantification of MYC protein expression in the depicted three primary-dispersed human PDAC cell lines. Each circle represents one biological replicate. Shown is the mean +/- SD.

D The growth inhibitory concentration 50% (GI_{50}) was determined for ML-93 and ML-792 in the depicted human primary dispersed PDAC lines. ATP (CellTiter-Glo®) was used as a surrogate to determine the dose-response of a seven-point dilution (ML-93: 0-1000 nM; ML-792: 0-5000 nM). Cells were treated for 72 hours. Assay was performed with at least three biological replicates conducted as technical triplicates. Shown is the mean +/- SD.

Biederstädt A, *et al. Gut* 2020;0:1–11. doi: 10.1136/gutjnl-2018-317856

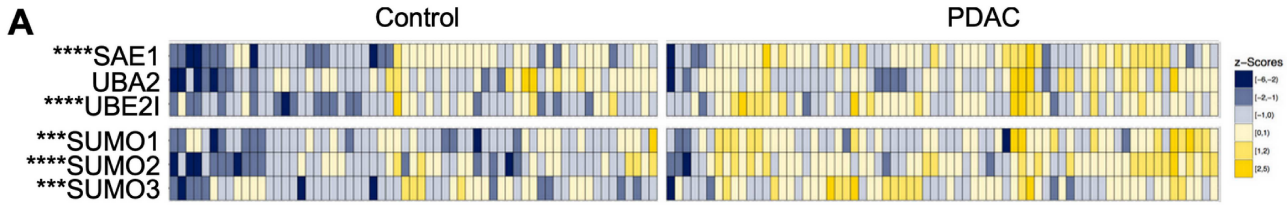
A
Control
PDAC
****SAE1
UBA2
****UBE2I
***SUMO1
****SUMO2
***SUMO3
z-Scores

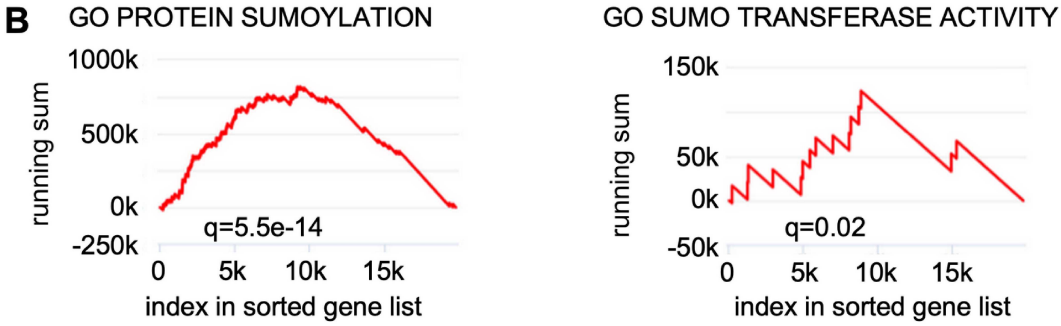
B
GO PROTEIN SUMOYLATION
GO SUMO TRANSFERASE ACTIVITY
running sum
index in sorted gene list
q=5.5e-14
q=0.02

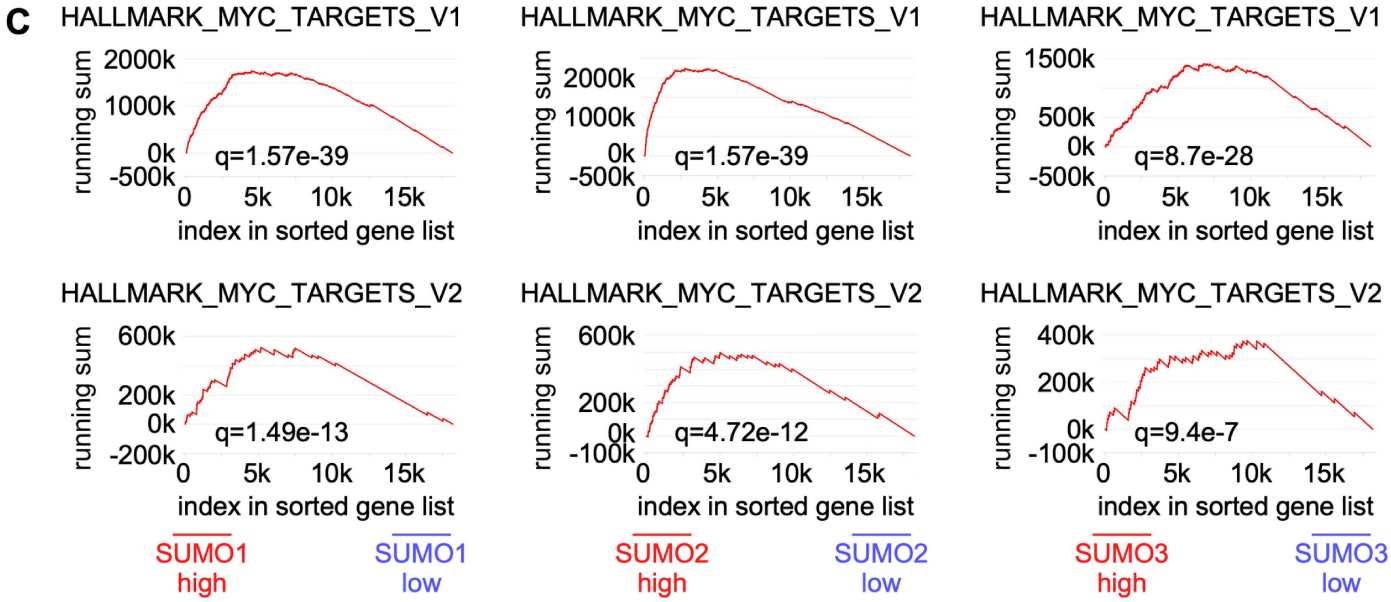
C
HALLMARK_MYC_TARGETS_V1
HALLMARK_MYC_TARGETS_V2
running sum
index in sorted gene list
q=1.57e-39
q=8.7e-28
q=1.49e-13
q=4.72e-12
q=9.4e-7
SUMO1 high
SUMO1 low
SUMO2 high
SUMO2 low
SUMO3 high
SUMO3 low

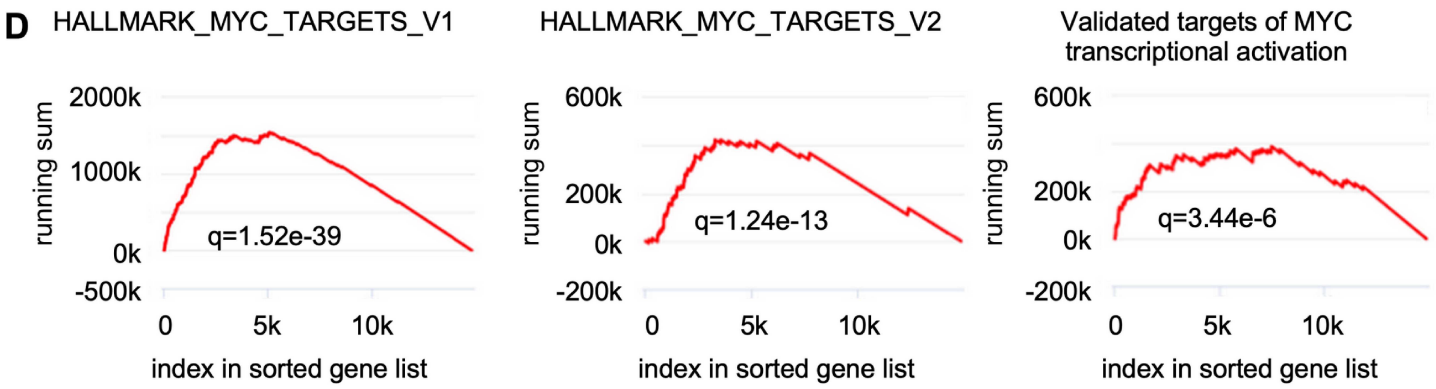
D
HALLMARK_MYC_TARGETS_V1
HALLMARK_MYC_TARGETS_V2
Validated targets of MYC transcriptional activation
running sum
index in sorted gene list
q=1.52e-39
q=1.24e-13
q=3.44e-6

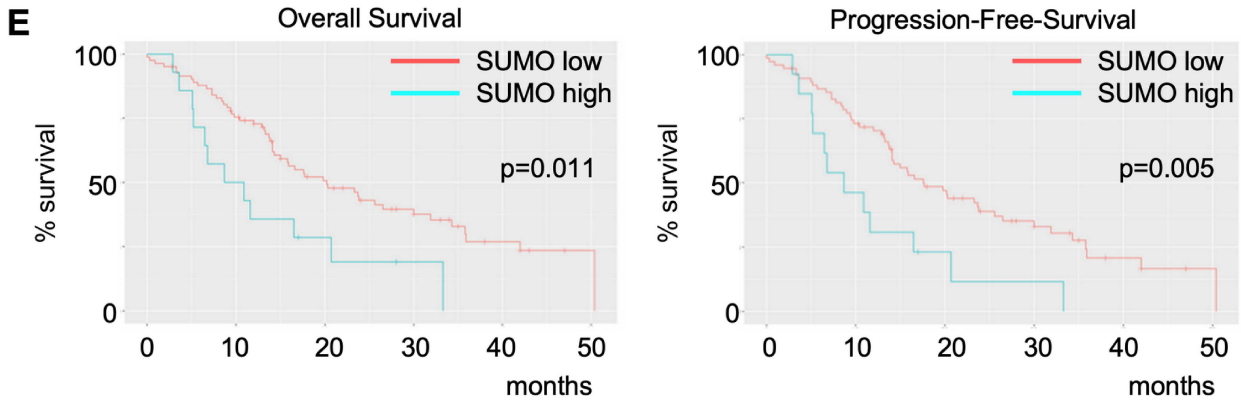
E
Overall Survival
Progression-Free-Survival
SUMO low
SUMO high
% survival
months
p=0.011
p=0.005

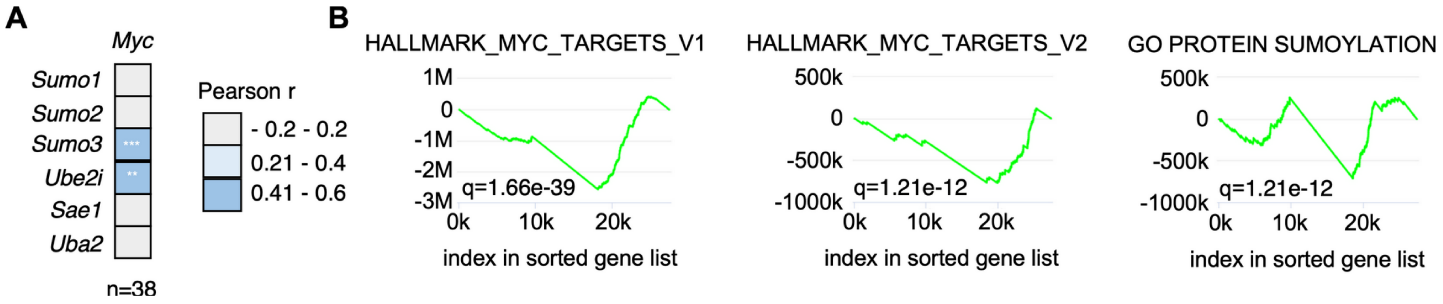
A
Myc
Sumo1
Sumo2
Sumo3
Ube2i
Sae1
Uba2
***
**
n=38
Pearson r
- 0.2 - 0.2
0.21 - 0.4
0.41 - 0.6
B
HALLMARK_MYC_TARGETS_V1
1M
0
-1M
-2M
-3M
q=1.66e-39
0k
10k
20k
index in sorted gene list
HALLMARK_MYC_TARGETS_V2
500k
0
-500k
-1000k
q=1.21e-12
0k
10k
20k
index in sorted gene list
GO PROTEIN SUMOYLATION
500k
0
-500k
-1000k
q=1.21e-12
0k
10k
20k
index in sorted gene list

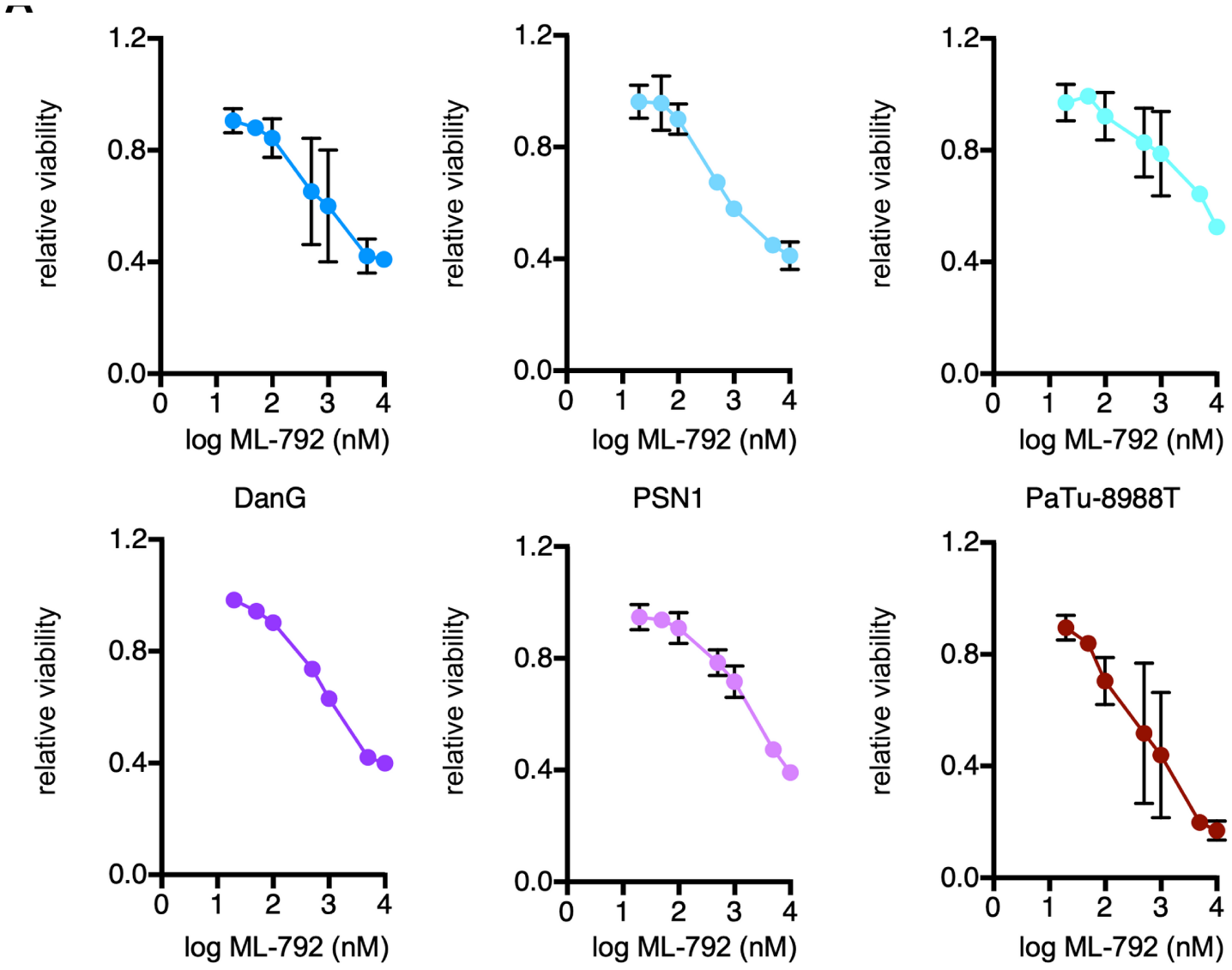
A
relative viability
log ML-792 (nM)
DanG
PSN1
PaTu-8988T
B
ML-93
ML-792
μM
0
0.0002
0.0007
0.0021
0.0062
0.0185
0.055
0.167
0.5
10
1
- UBC9-SUMO
- UBC9
- SUMO2/3 (conjugates)
- UBC12-NEDD8
- UBC12
- UBC10-Ub
- UBC10

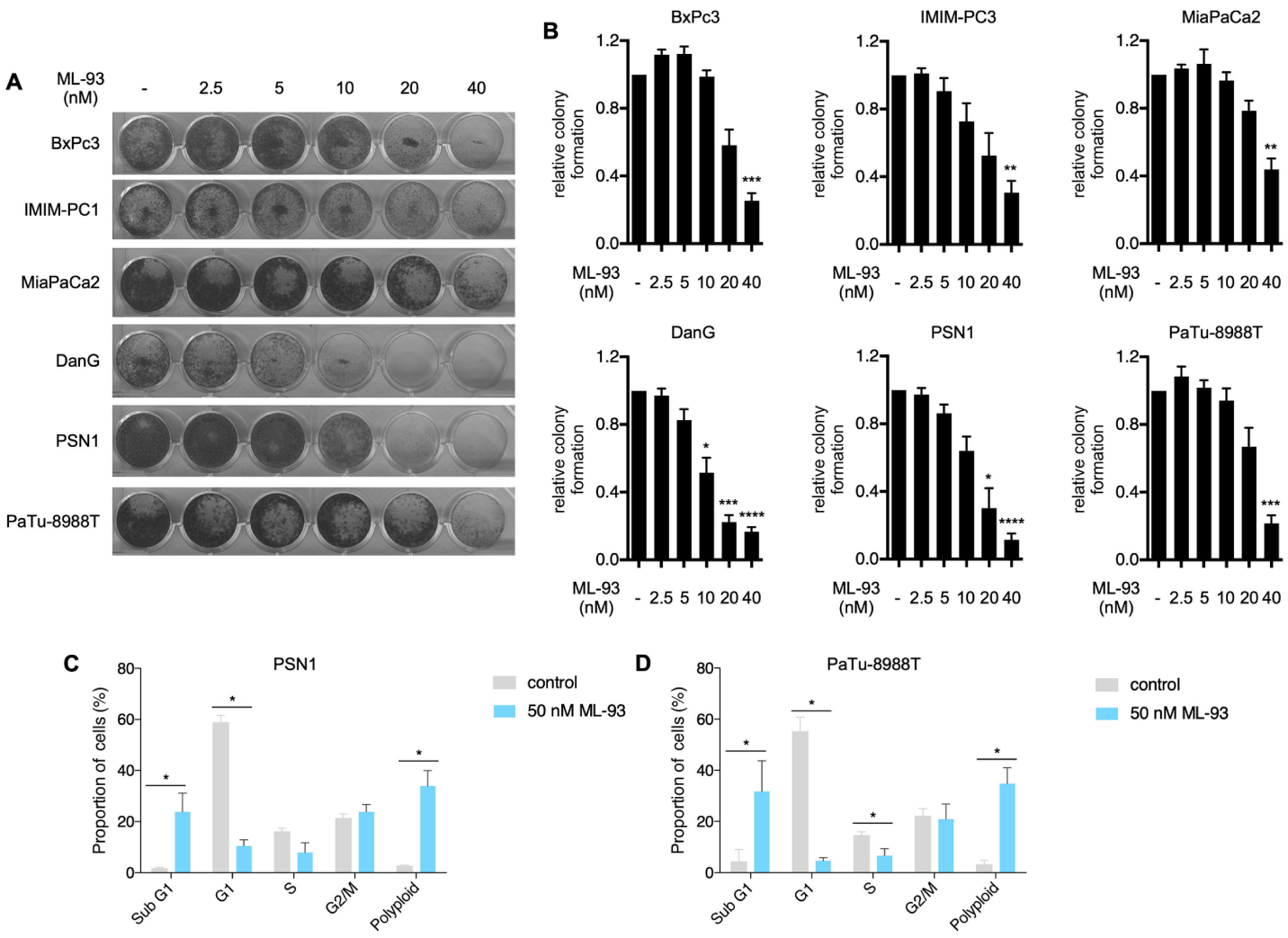
A
ML-93 (nM)
-
2.5
5
10
20
40
BxPc3
IMIM-PC1
MiaPaCa2
DanG
PSN1
PaTu-8988T
B
BxPc3
IMIM-PC3
MiaPaCa2
DanG
PSN1
PaTu-8988T
relative colony formation
ML-93 (nM)
C
PSN1
control
50 nM ML-93
Proportion of cells (%)
Sub G1
G1
S
G2/M
Polyploid
D
PaTu-8988T
control
50 nM ML-93
Proportion of cells (%)
Sub G1
G1
S
G2/M
Polyploid

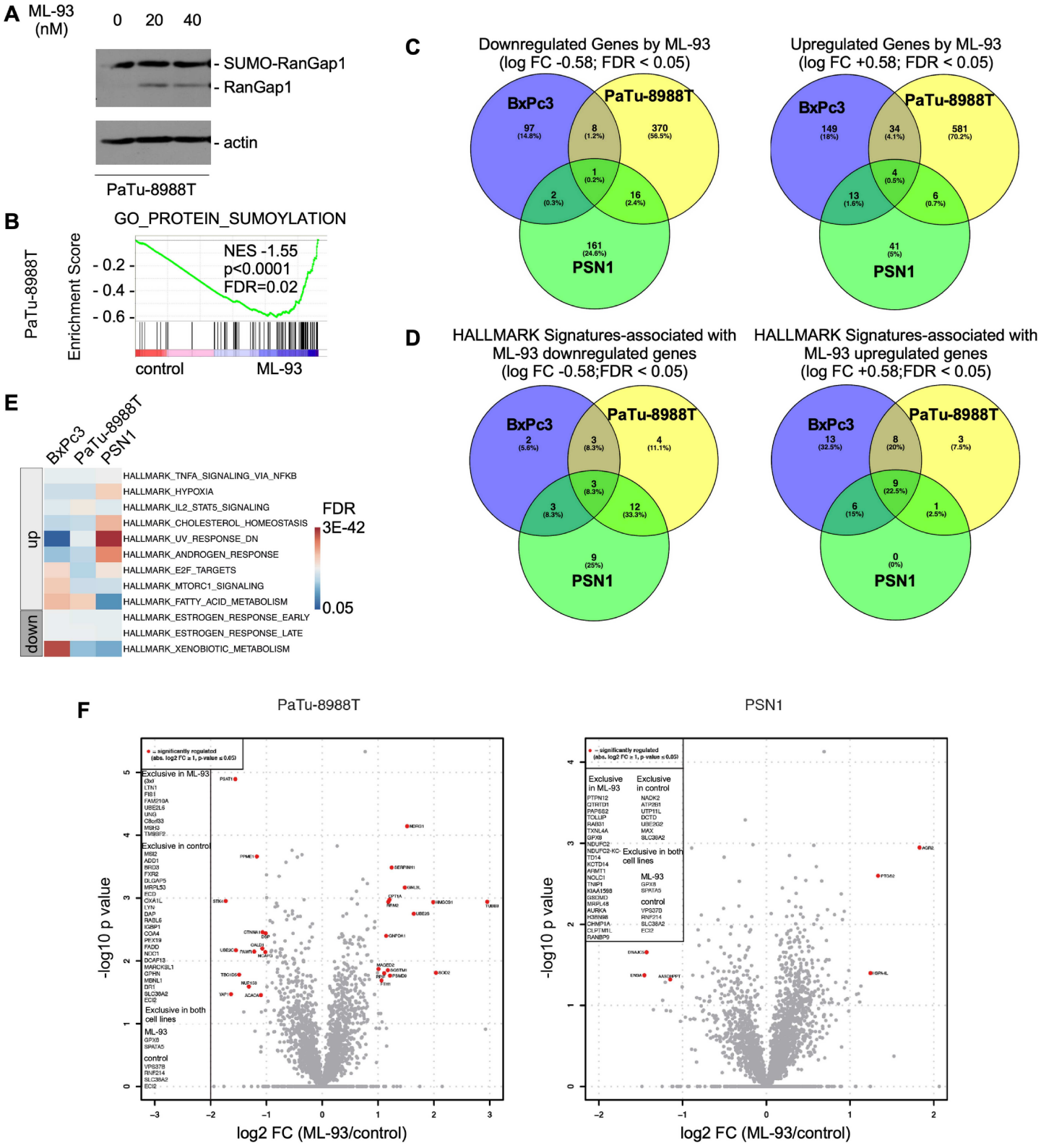
A
ML-93 (nM)
0 20 40
- SUMO-RanGap1
- RanGap1
- actin
PaTu-8988T
B
GO_PROTEIN_SUMOYLATION
PaTu-8988T
Enrichment Score
NES -1.55
p<0.0001
FDR=0.02
control
ML-93
C
Downregulated Genes by ML-93 (log FC -0.58; FDR < 0.05)
BxPc3
PaTu-8988T
PSN1
97 (14.8%)
8 (1.2%)
370 (56.5%)
1 (0.2%)
2 (0.3%)
16 (2.4%)
161 (24.6%)
Upregulated Genes by ML-93 (log FC +0.58; FDR < 0.05)
149 (18%)
34 (4.1%)
581 (70.2%)
4 (0.5%)
13 (1.6%)
6 (0.7%)
41 (5%)
D
HALLMARK Signatures-associated with ML-93 downregulated genes (log FC -0.58;FDR < 0.05)
2 (5.6%)
3 (8.3%)
4 (11.1%)
3 (8.3%)
3 (8.3%)
12 (33.3%)
9 (25%)
HALLMARK Signatures-associated with ML-93 upregulated genes (log FC +0.58;FDR < 0.05)
13 (32.5%)
8 (20%)
3 (7.5%)
9 (22.5%)
6 (15%)
1 (2.5%)
0 (0%)
E
BxPc3
PaTu-8988T
PSN1
up
down
HALLMARK_TNFA_SIGNALING_VIA_NFKB
HALLMARK_HYPOXIA
HALLMARK_IL2_STAT5_SIGNALING
HALLMARK_CHOLESTEROL_HOMEOSTASIS
HALLMARK_UV_RESPONSE_DN
HALLMARK_ANDROGEN_RESPONSE
HALLMARK_E2F_TARGETS
HALLMARK_MTORC1_SIGNALING
HALLMARK_FATTY_ACID_METABOLISM
HALLMARK_ESTROGEN_RESPONSE_EARLY
HALLMARK_ESTROGEN_RESPONSE_LATE
HALLMARK_XENOBIOTIC_METABOLISM
FDR
3E-42
0.05
F
PaTu-8988T
PSN1
-log10 p value
log2 FC (ML-93/control)
Exclusive in ML-93
Exclusive in control
Exclusive in both cell lines
ML-93
control

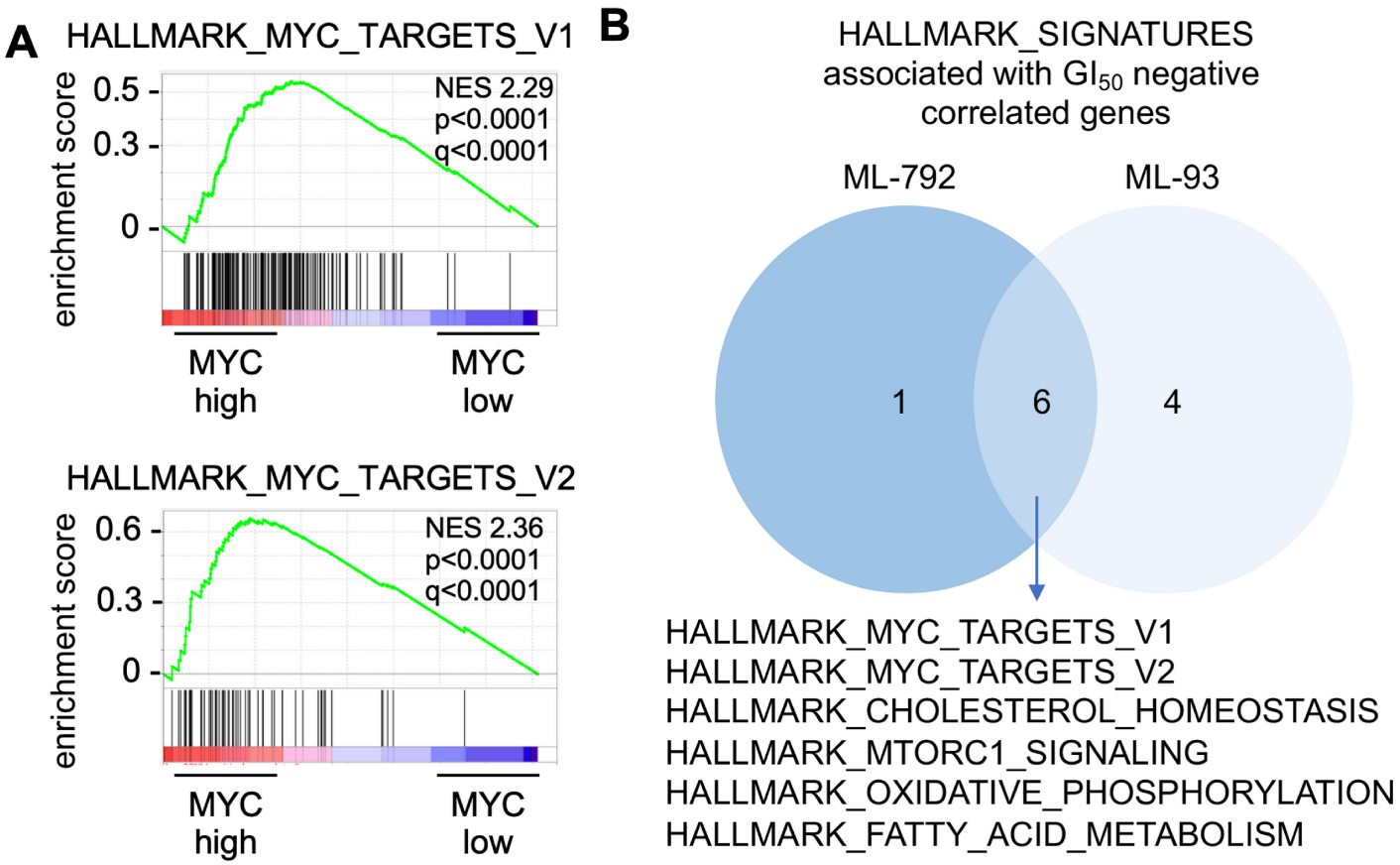
A
HALLMARK_MYC_TARGETS_V1
enrichment score
0.5
0.3
0
NES 2.29
p<0.0001
q<0.0001
MYC high
MYC low
HALLMARK_MYC_TARGETS_V2
enrichment score
0.6
0.3
0
NES 2.36
p<0.0001
q<0.0001
MYC high
MYC low
B
HALLMARK_SIGNATURES
associated with GI50 negative
correlated genes
ML-792
ML-93
1
6
4
HALLMARK_MYC_TARGETS_V1
HALLMARK_MYC_TARGETS_V2
HALLMARK_CHOLESTEROL_HOMEOSTASIS
HALLMARK_MTORC1_SIGNALING
HALLMARK_OXIDATIVE_PHOSPHORYLATION
HALLMARK_FATTY_ACID_METABOLISM

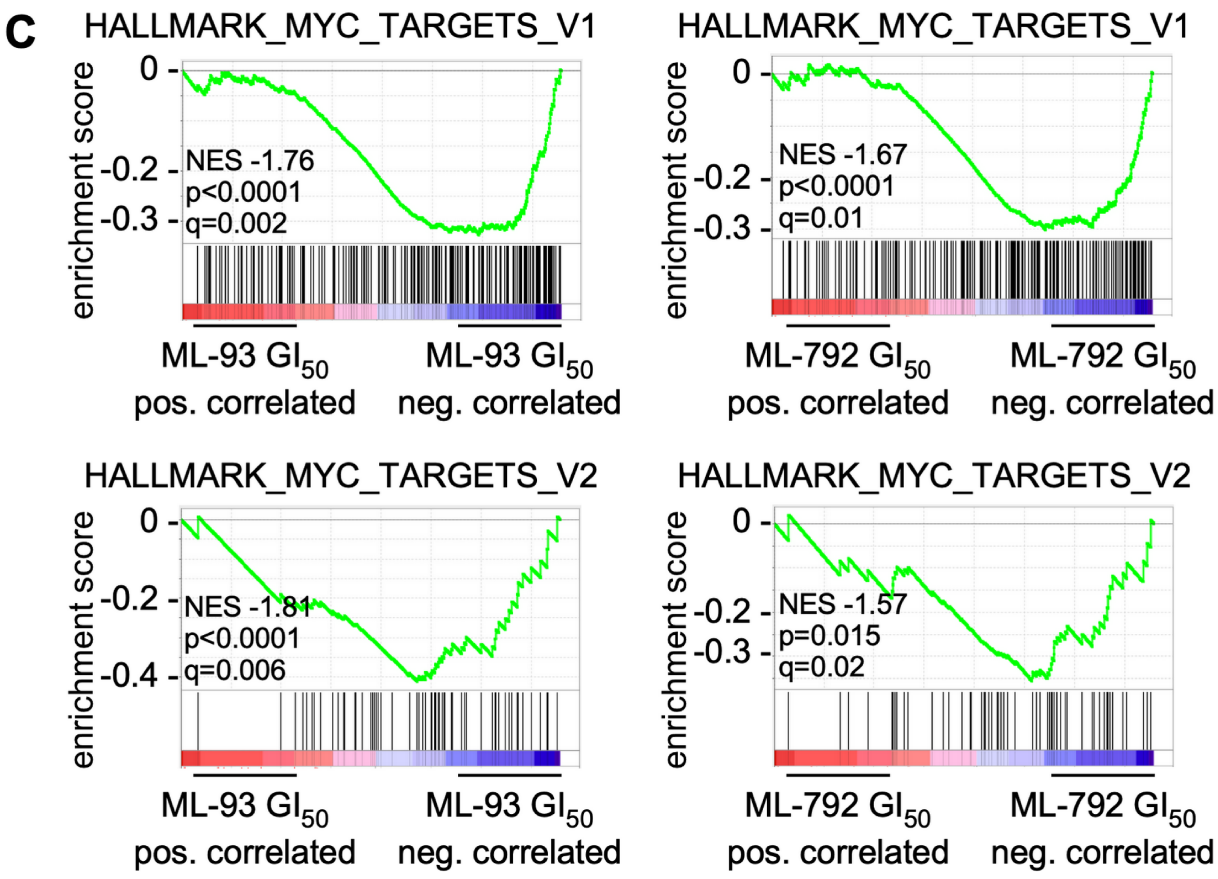
C
HALLMARK_MYC_TARGETS_V1
enrichment score
0
-0.2
-0.3
NES -1.76
p<0.0001
q=0.002
ML-93 GI50 pos. correlated
ML-93 GI50 neg. correlated
HALLMARK_MYC_TARGETS_V1
enrichment score
0
-0.2
-0.3
NES -1.67
p<0.0001
q=0.01
ML-792 GI50 pos. correlated
ML-792 GI50 neg. correlated
HALLMARK_MYC_TARGETS_V2
enrichment score
0
-0.2
-0.4
NES -1.81
p<0.0001
q=0.006
ML-93 GI50 pos. correlated
ML-93 GI50 neg. correlated
HALLMARK_MYC_TARGETS_V2
enrichment score
0
-0.2
-0.3
NES -1.57
p=0.015
q=0.02
ML-792 GI50 pos. correlated
ML-792 GI50 neg. correlated

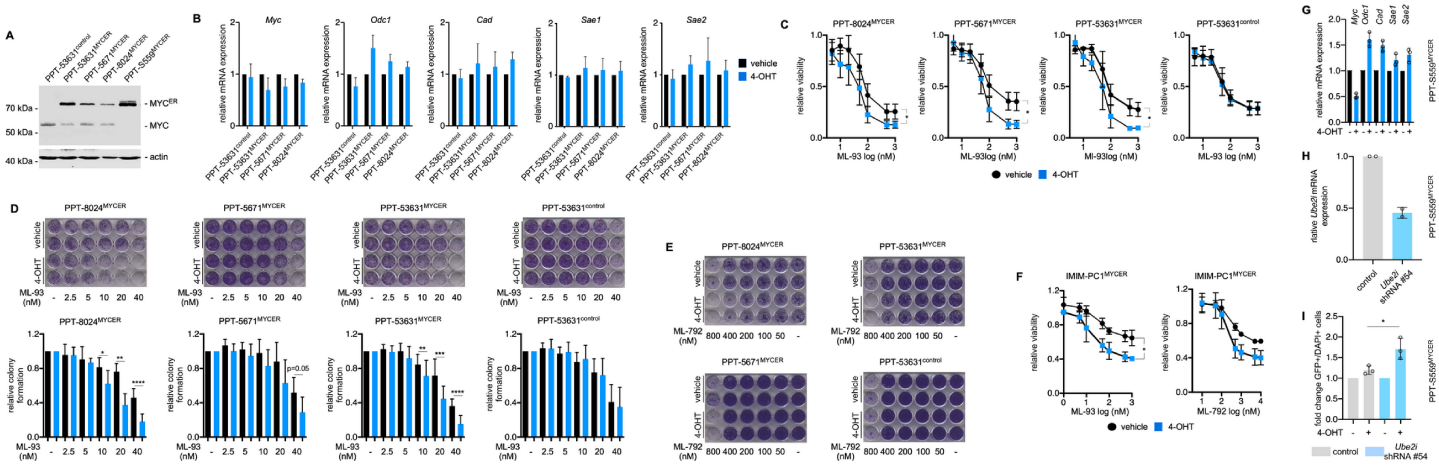
A
PPT-53631control
PPT-53631MYCER
PPT-5671MYCER
PPT-8024MYCER
PPT-5559MYCER
70 kDa -
50 kDa -
40 kDa -
- MYCER
- MYC
- actin
B
Myc
Odc1
Cad
Sae1
Sae2
relative mRNA expression
vehicle
4-OHT
C
PPT-8024MYCER
PPT-5671MYCER
PPT-53631MYCER
PPT-53631control
relative viability
ML-93 log (nM)
vehicle
4-OHT
D
PPT-8024MYCER
PPT-5671MYCER
PPT-53631MYCER
PPT-53631control
vehicle
4-OHT
ML-93 (nM)
relative colony formation
p=0.05
E
PPT-8024MYCER
PPT-53631MYCER
PPT-5671MYCER
PPT-53631control
ML-792 (nM)
F
IMIM-PC1MYCER
relative viability
ML-93 log (nM)
ML-792 log (nM)
vehicle
4-OHT
G
Myc
Odc1
Cad
Sae1
Sae2
relative mRNA expression
PPT-5559MYCER
4-OHT
H
relative Ube2i mRNA expression
PPT-5559MYCER
control
Ube2i shRNA #54
I
fold change GFP+/DAPI+ cells
PPT-5559MYCER
4-OHT
control
Ube2i shRNA #54

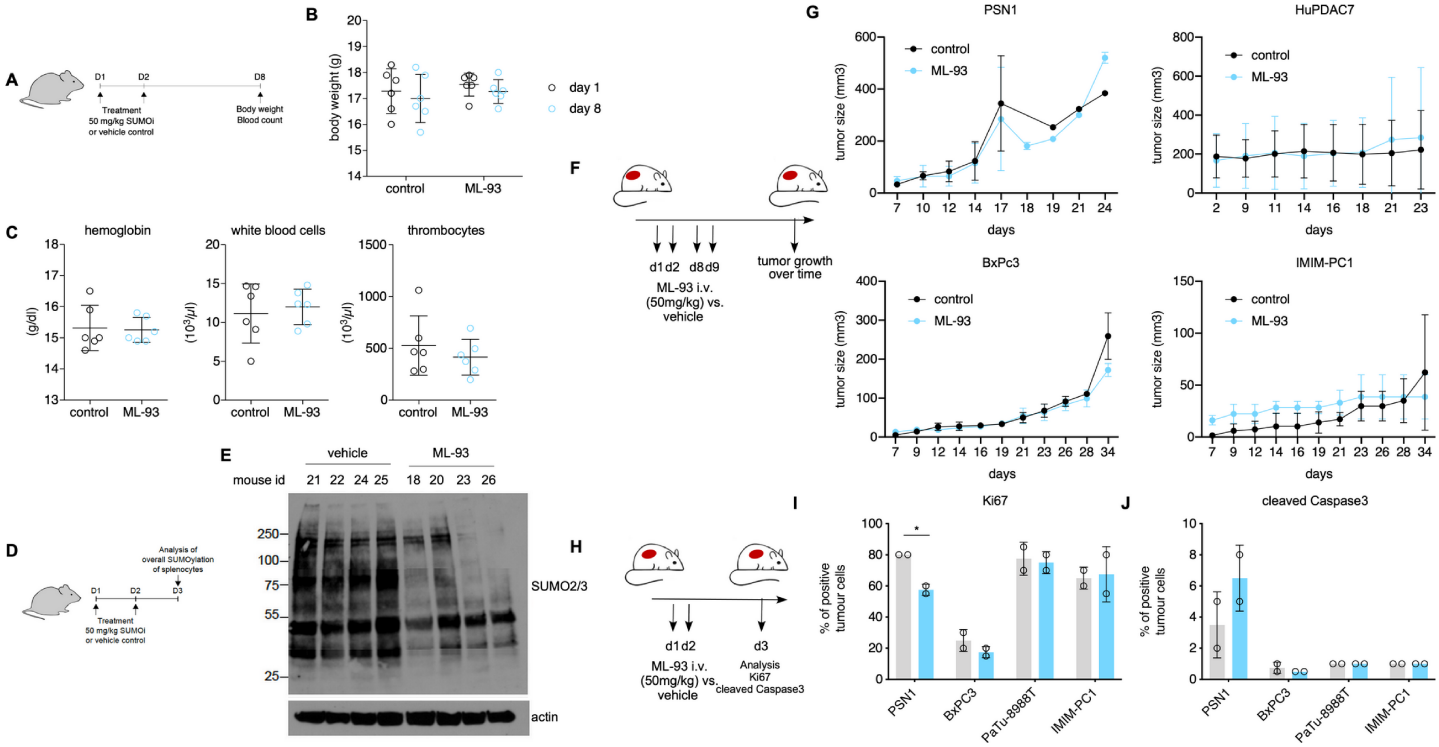
A
D1
D2
D8
Treatment
50 mg/kg SUMOi
or vehicle control
Body weight
Blood count
B
body weight (g)
control
ML-93
day 1
day 8
C
hemoglobin
white blood cells
thrombocytes
(g/dl)
(10³/µl)
control
ML-93
D
Analysis of
overall SUMOylation
of splenocytes
Treatment
50 mg/kg SUMOi
or vehicle control
E
vehicle
ML-93
mouse id
21 22 24 25
18 20 23 26
250
100
75
55
25
SUMO2/3
actin
F
d1 d2
d8 d9
ML-93 i.v.
(50mg/kg) vs.
vehicle
tumor growth
over time
G
PSN1
HuPDAC7
BxPc3
IMIM-PC1
control
ML-93
tumor size (mm3)
days
H
d1 d2
d3
ML-93 i.v.
(50mg/kg) vs.
vehicle
Analysis
Ki67
cleaved Caspase3
I
Ki67
% of positive
tumour cells
PSN1
BxPC3
PaTu-8988T
IMIM-PC1
J
cleaved Caspase3
% of positive
tumour cells
PSN1
BxPC3
PaTu-8988T
IMIM-PC1

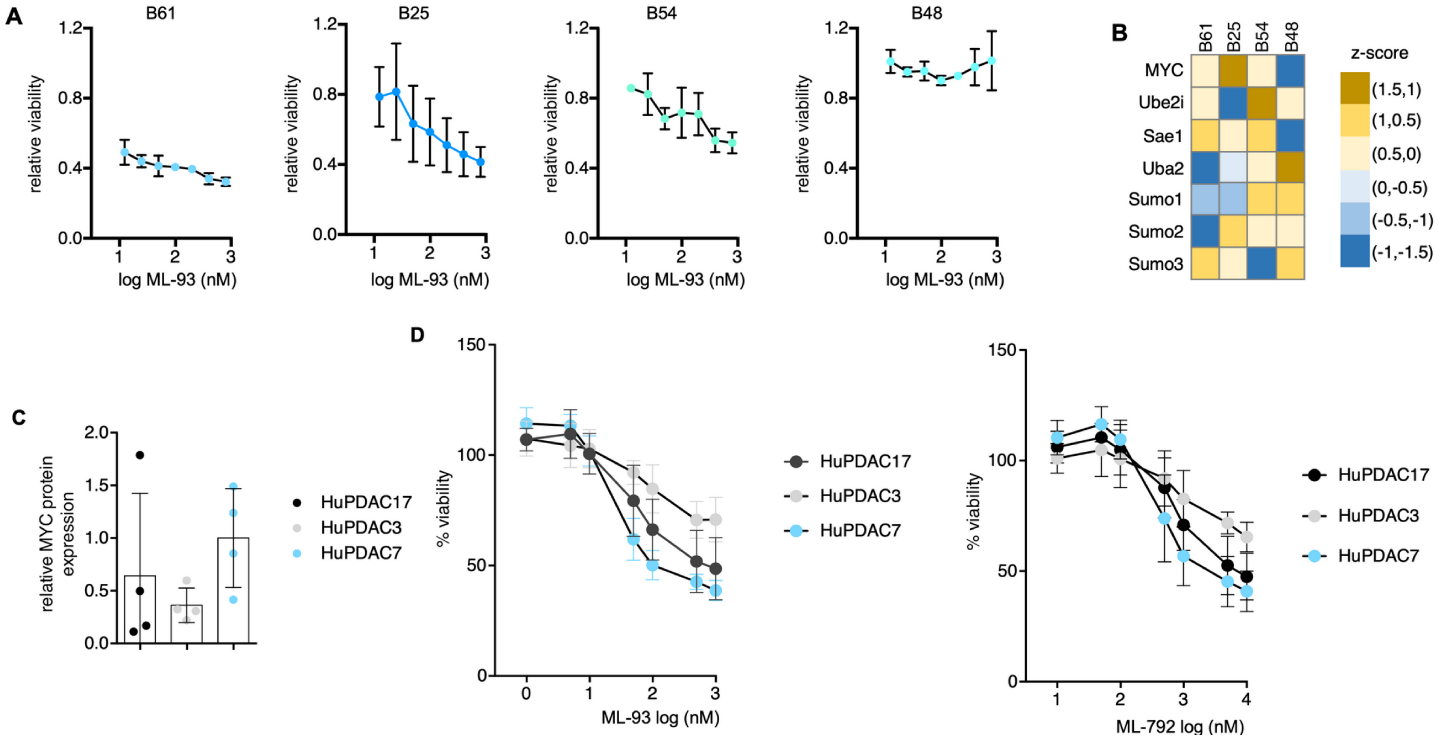
A
B61
B25
B54
B48
relative viability
log ML-93 (nM)
B
MYC
Ube2i
Sae1
Uba2
Sumo1
Sumo2
Sumo3
z-score
(1.5,1)
(1,0.5)
(0.5,0)
(0,-0.5)
(-0.5,-1)
(-1,-1.5)
C
relative MYC protein expression
HuPDAC17
HuPDAC3
HuPDAC7
D
% viability
ML-93 log (nM)
ML-792 log (nM)